
Remote sensing and GIS for mapping groundwater recharge and discharge areas in salinity prone catchments, southeastern Australia

Sarah O. Tweed · Marc Leblanc · John A. Webb · Maciek W. Lubczynski

Abstract Identifying groundwater recharge and discharge areas across catchments is critical for implementing effective strategies for salinity mitigation, surface-water and groundwater resource management, and ecosystem protection. In this study, a synergistic approach has been developed, which applies a combination of remote sensing and geographic information system (GIS) techniques to map groundwater recharge and discharge areas. This approach is applied to an unconfined basalt aquifer, in a salinity and drought prone region of southeastern Australia. The basalt aquifer covers ~11,500 km² in an agriculturally intensive region. A review of local hydrogeological processes allowed a series of surface and subsurface indicators of groundwater recharge and discharge areas to be established. Various remote sensing and GIS techniques were then used to map these surface indicators including: terrain analysis, monitoring of vegetation activity, and mapping of infiltration capacity. All regions where groundwater is not discharging to the surface were considered potential recharge areas. This approach, applied systematically across a catchment, provides a framework for mapping recharge and discharge areas. A key component in assigning surface and subsurface indicators is the relevance to the dominant recharge and discharge processes occurring and the use of appropriate remote sensing and GIS techniques with the capacity to identify these processes.

Résumé Sur un bassin versant, l'identification des zones d'alimentation et des aires d'émergence des eaux souterraines est capitale pour mettre en œuvre des stratégies de réduction de la salinité, de gestion des eaux souterraines et superficielles, et de protection des écosystèmes. Une approche synergique a été développée, sur la base de recherches existantes pour cartographier de manière systématique les zones de recharge et d'émergence. Elle combine des techniques de télédétection et de Systèmes d'Information Géographique, dans le but de cartographier les zones d'alimentation et d'émergence. Ces techniques ont été appliquées à un aquifère basaltique libre, dans un secteur sujet à la sécheresse et à la salinité du Sud-Est australien. L'aquifère considéré couvre environ 11,500 km² d'une région essentiellement agricole. Un inventaire des processus hydrogéologiques locaux a conduit à l'établissement d'une série d'indicateurs superficiels et sub-superficiels des zones d'alimentation et d'émergence. Plusieurs méthodes de télédétection et de SIG furent alors utilisées pour cartographier ces indicateurs de surface, y compris les analyses de terrain, le suivi de l'activité de la végétation et la cartographie des capacités d'infiltration. Toutes les régions en dehors des zones d'émergence sont considérées comme des zones d'alimentation potentielles. Un des composants clés de l'attribution des indicateurs superficiels et subsuperficiels est la concordance avec les processus majeurs d'alimentation et de prélèvement entrant en jeu, et l'utilisation de méthodes de télédétection et SIG adaptées permettant d'identifier ces processus.

Resumen La identificación de áreas de descarga y recarga de agua subterránea es crítica para la implementación de estrategias efectivas relacionadas con mitigación de salinidad, gestión de recursos de agua subterránea y agua superficial, y protección de ecosistemas. En este estudio se ha desarrollado un enfoque sinérgico apoyándose en investigación existente el cual aplica una combinación de técnicas de sistemas de información geográfico (SIG) y sensores remotos para cartografiar áreas de recarga y descarga de agua subterránea. Este enfoque se aplica a un acuífero de basalto no confinado en una región del sureste de Australia propensa a sequía y salinidad. El acuífero de basalto cubre aproximadamente 11,500 km² en una región con agricultura intensiva. Una revisión de los procesos hidrogeológicos locales permitió el establecimiento de una serie de indicadores superficiales y subterráneos de áreas

Received: 13 April 2006 / Accepted: 25 October 2006

© Springer-Verlag 2006

S. O. Tweed (✉) · M. Leblanc
School of Geosciences, Monash University,
Melbourne, VIC 3800, Australia
e-mail: sarah.tweed@sci.monash.edu.au
Tel.: +61-3-99053097
Fax: +61-3-99054903

J. A. Webb
Department of Earth Sciences, La Trobe University,
Bundoora, VIC 3086, Australia

M. W. Lubczynski
Department of Water Resources, ITC,
Enschede, 7500 AA, The Netherlands

de recarga y descarga de agua subterránea. Luego se utilizaron varias técnicas de SIG y sensores remotos para cartografiar estos indicadores superficiales incluyendo: análisis del terreno, monitoreo de la actividad de la vegetación, y cartografiado de la capacidad de infiltración. Todas las regiones donde el agua subterránea no descarga en la superficie fueron consideradas áreas potenciales de recarga. Este enfoque que se ha aplicado sistemáticamente a través de la cuenca aporta un marco para la cartografía de áreas de recarga y descarga. Un componente clave en la asignación de indicadores superficiales y subterráneos lo constituye la relevancia a los procesos dominantes de recarga y descarga que ocurren y el uso de técnicas apropiadas de SIG y sensores remotos con la capacidad para identificar esos procesos.

Keywords Geographic information system · Satellite imagery · Terrain analysis · Groundwater recharge/discharge · Salinisation

Introduction

In salinity prone catchments, effective management of water resources involves balancing the requirements of sustainable resource allocation with salinity mitigation programs and ecosystem protection. Understanding groundwater recharge and discharge processes is a key component to achieving this balance. Surface water and groundwater resource allocation requires knowledge of the areal extent and processes controlling the influx, including preferential recharge areas, and outflux via direct discharge, transpiration, and evaporation. In large regions of Australia, evapotranspiration during groundwater recharge and discharge is also integral to controls on increased salinisation of land and water resources. Evapotranspiration of rainfall during relatively slow recharge (Herczeg et al. 2001), and of shallow water tables (Cartwright et al. 2004), results in increased groundwater salinity. On the other hand, groundwater transpiration by vegetation and direct discharge to wetlands and rivers, means that shallow water tables are an essential component of sustaining ecologically significant areas (Batelaan et al. 2003).

To define the spatial extent of recharge and discharge processes occurring across a catchment, a synergistic approach is most effective, as controls on these processes vary in scale and location due to changes in terrain, geology, hydrogeological regimes, and climate. Field methods are available to investigate the spatio-temporal variability of recharge and discharge processes (Kishel and Gerla 2002), but typically they are site-specific, i.e. restricted to local scale of investigation. The most important advantage of using satellite-derived data in identifying hydrogeological processes refers to the spatially extensive, multi-temporal, and cost-effective data coverage (Rango and Shalaby 1998; Bastiaanssen et al. 2000; Hoffmann 2005). Therefore, provided remote sensing data can effectively contribute to the hydrogeological investigation, such datasets are particularly useful

when large areas have to be investigated and on-ground data are sparse and/or difficult to access.

Taking examples from one study area, this paper proposes a systematic and synergistic approach to mapping groundwater recharge and discharge areas across a regional unconfined aquifer. A series of surface and subsurface indicators are chosen to identify recharge and discharge areas. This approach uses a combination of different remote sensing and geographic information system (GIS) techniques, which require the integration of multiple datasets, including GIS (soil map, digital elevation model (DEM), groundwater electrical conductivity (EC), flow, and depth to water-table maps) and remote-sensing data (Landsat, airborne radiometrics, and aerial photos).

Brief literature review

Many hydrogeological applications of remote sensing rely on the user to link image or data interpretation to groundwater processes (Meijerink 1996). For example, in many semi-arid areas, discharge of groundwater to the surface results in soil salinisation and growth of salt-tolerant vegetation. There are many different remote-sensing techniques for monitoring salinity-affected soil and vegetation, i.e. aerial photographs, video images, infrared thermography, microwave and hyperspectral sensing, airborne geophysics and electromagnetic induction (Metternicht and Zinck 2003). These techniques, which require on-ground data to infer the effect of groundwater discharge, have been used in many studies to identify vegetation type or soil condition (Meijerink 1996; Metternicht and Zinck 1997; Dehaan and Taylor 2002; McFarlane and Williamson 2002; Howari 2003; Spies and Woodgate 2005). Remote-sensing techniques using Landsat (TM and ETM+) have also been used to identify groundwater discharge areas by identifying changes in lakes temperature (Tcherepanov et al. 2005), and by mapping lineaments associated with groundwater springs (Sener et al. 2005).

Remote-sensing data can also be used to determine the distribution of recharge by the identification of near-surface parameters. For example, Bierwirth and Welsh (2000) mapped aquifers using airborne radiometric images, and from this delineated the extent of unconfined aquifers that were preferentially recharged. Microwave remote sensing of soil moisture has also been used to determine soil hydraulic properties for recharge estimates (Jackson 2002). A GIS cross-overlay procedure can be used to merge different component maps and weight information relating to controls on recharge processes (Lubczynski and Gurwin 2005). The mapping of relative recharge rates has been applied to studies in aquifer vulnerability modelling, i.e. using the DRASTIC approach (Fritch et al. 2000; Al-Adamat et al. 2003), and as input information for numerical modelling (Salama et al. 1999; Lubczynski and Gurwin 2005).

To identify both recharge and discharge areas within a catchment, other investigations have also synergistically applied on-ground data with remote sensing and GIS

techniques to link surface features with groundwater processes. This approach requires integration of the satellite data with catchment data within a GIS framework (Meijerink 1996). A study by Bobba et al. (1992) used Landsat data to identify recharge and discharge areas by the changes in near-surface temperature and thereby related this to spring water-table elevations. Salama et al. (1994) integrated the interpretation of geomorphic and geological features, from Landsat-TM and aerial photographs, with on-ground hydrogeological studies to map recharge and discharge areas. They found recharge areas were linked to increases in permeability of the surficial geology, whereas discharge areas were associated with major drainage lines, geological boundaries, and topographic depressions. Leblanc et al. (2003a,b) also highlighted the use of remote sensing (Meteosat thermal, Landsat optical and Modis normalized vegetation index (NDVI) data) and GIS (DEM, soil map, and depth to the water table) data to identify land-surface features that control or originate from the location of groundwater recharge and discharge areas in a large data-scarce, semi-arid basin.

Study area

Geography and hydrogeology

The study area is located in a regional surface-water catchment known as the Glenelg-Hopkins catchment, located in southeastern Australia (Fig. 1a). In this study, hydrogeological processes occurring within the unconfined Newer Volcanics basalt aquifer were investigated. The aquifer underlies the eastern half of the regional surface water catchment (Fig. 1a). The basalt aquifer covers an area of approximately 11,500 km² (46% of the Glenelg-Hopkins surface water catchment). The basalt aquifer is essentially covered by agricultural land use with very little remnant vegetation (Eucalyptus forest) remaining. Dryland pasture makes up the bulk of agricultural activity, however, dryland cropping and blue gum industries have significantly expanded in recent years at the expense of grazing (Ierodiaconou et al. 2005). The study area is exposed to an ocean-influenced climate in the south, resulting in greater rainfall compared to the northern region (Fig. 2).

The surface elevation of the basalt aquifer region decreases from north to south. However, except for a small area in the northeast, the basalt aquifer is largely flat with gentle undulations—from 0 to 300 metres above Australian Height Datum (mAHD). Stream networks drain to the south (Fig. 1a), and wetlands locally occupy topographic depressions in the landscape. Of the 3,000 lakes and wetlands located in the basalt region the wetland types include freshwater meadows (55%), shallow and deep freshwater marshes (15 and 7% respectively), permanent open freshwater (14%), and semi-permanent and permanent saline wetlands (7 and 1% respectively). Most lakes and wetlands are shallow with small drainage

networks, so that groundwater is considered an important component sustaining the water levels during summer.

The basalt aquifer consists of tholeiitic lava flows ranging in age between ~4 and ~0.3 Ma (10⁶ years), and are typically 30–40 m thick (Bennetts et al. 2006). The age variations have resulted in different thicknesses and clay content of the weathering profiles, which, therefore, alters the hydraulic connectivity among the different basalt flows. The differences in weathering profiles affect vertical infiltration properties of the shallow zone, which is explored further below.

Within the basalt aquifer, groundwater potentiometric contours indicate regional flow towards the south (Fig. 1b); however, groundwater is also locally recharged and discharged throughout the region. The average depth to water table in the basalt aquifer ranges predominantly between 0 and 30 m and higher values are mostly observed in the southern region. Average groundwater EC varies considerably from <1,000 to >100,000 $\mu\text{S}/\text{cm}$ (Fig. 1c). The salinisation processes within the study area are similar to those impacting water resources throughout southeastern Australia, where evapotranspiration of infiltrating rainfall and shallow water tables results in increased groundwater salinity (Herczeg et al. 2001). Catchment management issues within the study area include impacts from dryland salinity processes on land and water resources, and preservation of groundwater dependent ecosystems. Thus, delineation of recharge and discharge areas, particularly when affected by salinisation processes, is a key component to effective groundwater management.

Discharge processes

Groundwater discharge processes within the study area include evaporation and transpiration of groundwater, and groundwater flow to the surface, including discharge to wetlands, lakes, rivers, and the ocean.

In many regions of southeastern Australia, the replacement of deep-rooted perennial native vegetation with shallow-rooted annual crops has resulted in a general rise of water tables (Allison et al. 1990), and, therefore, increased discharge to the surface and via evaporation. As well as changes in water-table depths, the evaporation rate can vary considerably under different climate regimes and for soils with different hydraulic conductivities (Thorburn et al. 1992; Salama 1998; Gowing et al. 2006). In semi-arid areas, for soils ranging from sandy to clay-rich, significant evaporation of groundwater from up to 5 m depth has been reported by Salama (1998), and Lubczynski and Gurwin (2005). Therefore, within the study area which has a more humid environment, a depth to water table of <5 m can be assumed as a limit for significant groundwater evaporation.

The annual soil-water deficit is greatest during summer in the sub-humid, northern region of the study area, where the average aridity index (AI=annual rainfall/potential evapotranspiration; UNEP 1992), varies between 0.55 and 0.65 (Fig. 2). In this region, rainfall is the limiting factor

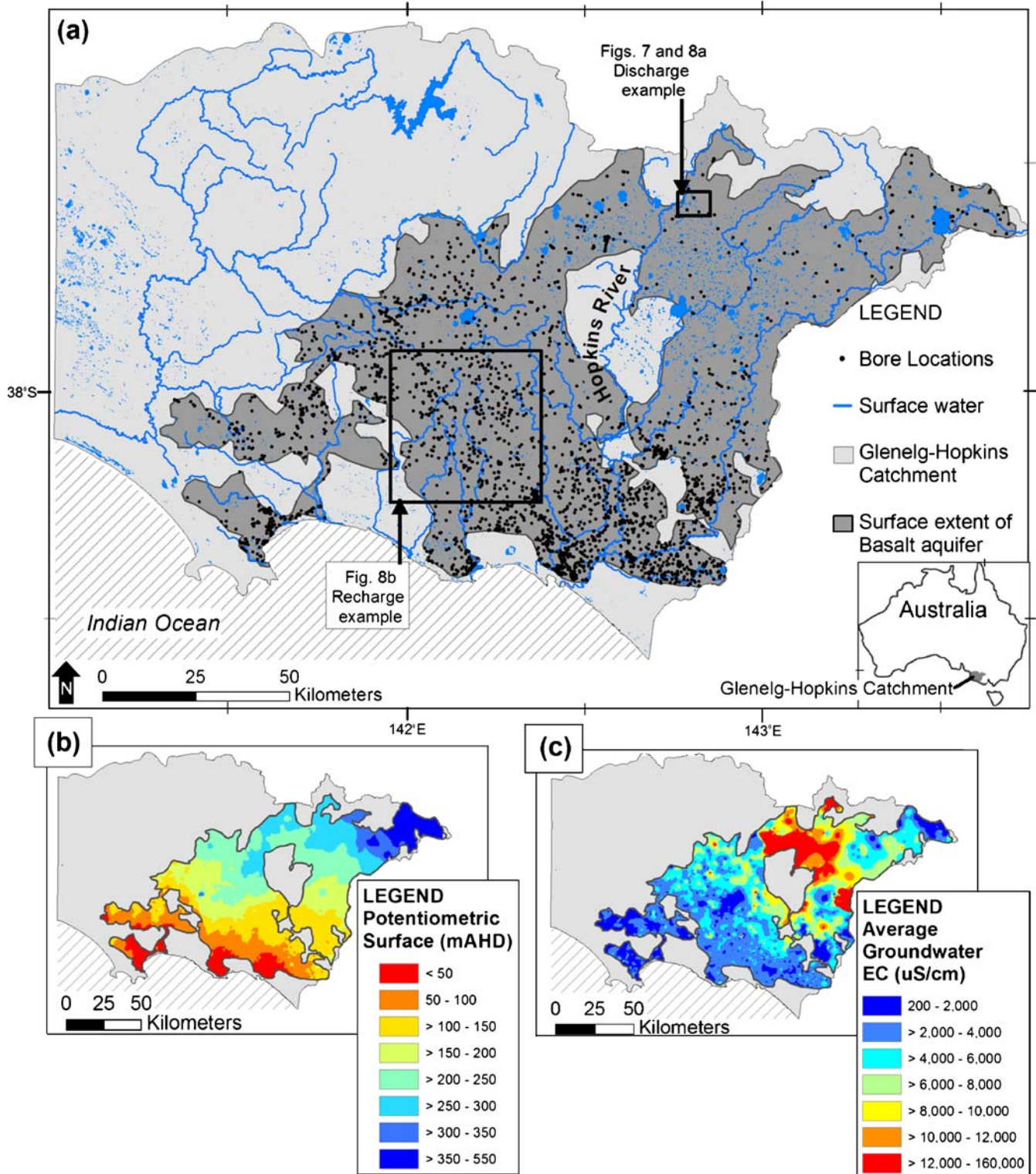


Fig. 1 a Location of the basalt aquifer, bores, and surface-water within the study area in southeastern Australia. The b potentiometric surface and c groundwater electrical conductivity (EC) for the basalt aquifer

for the local vegetation growth during the summer. Where fresh groundwater discharge occurs, the constant availability of water sustains plant photosynthetic activity longer into the summer. Approximately 140 km² of the basalt aquifer (~1.2% of the total aquifer area), has soil

and/or vegetation species affected by salinisation processes (Munro 2000). Because the region is predominantly devoted to agricultural land uses, areas where shallow saline groundwater is close to, or discharges to the surface, are also evident from the vegetation activity.

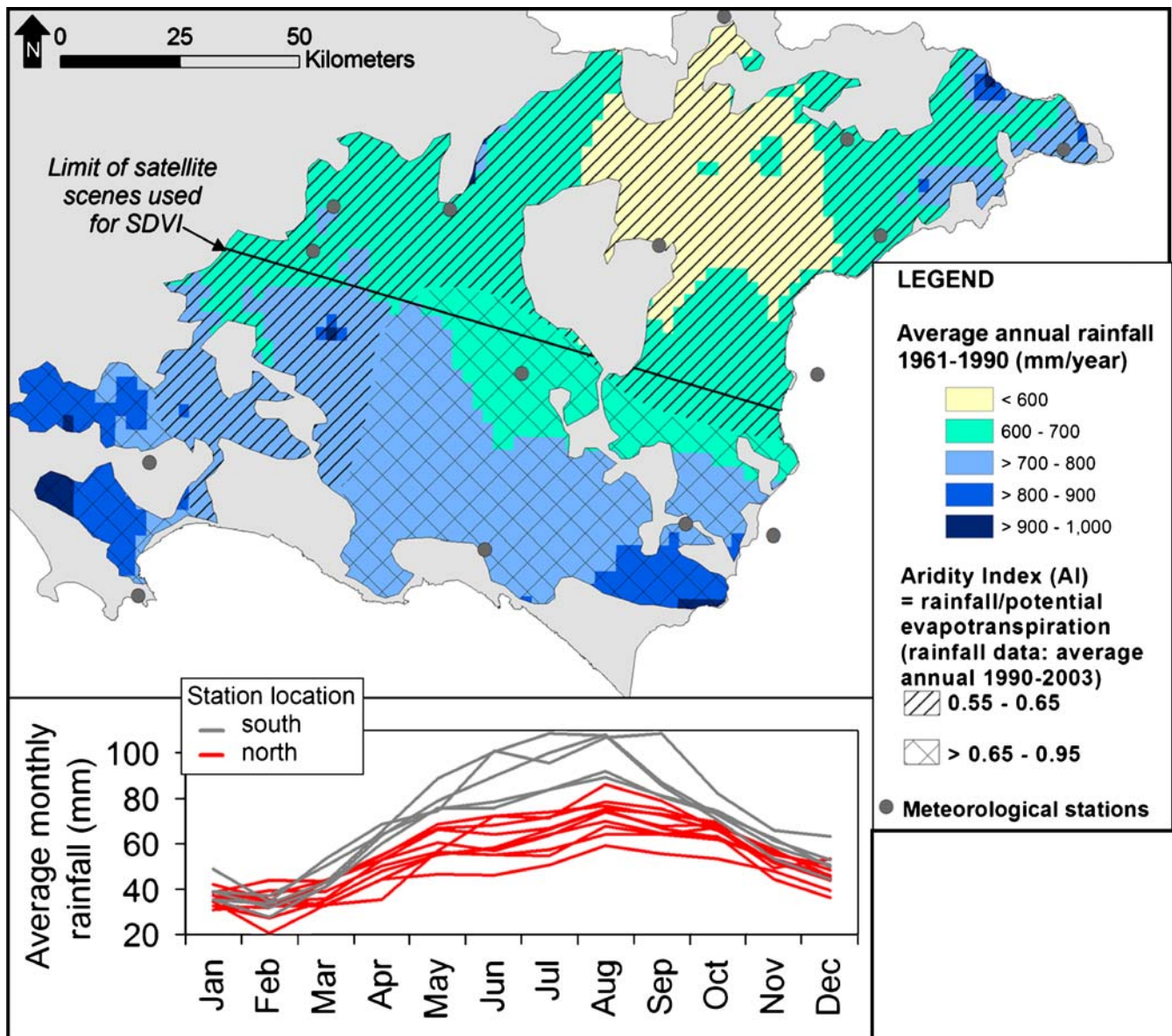


Fig. 2 Rainfall and aridity index. The line drawn showing the limit of the satellite scenes approximately divides the northern and southern regions

Where saline groundwater discharge occurs, salt accumulation limits photosynthetic activity throughout the year, or the saline groundwater supports salt-tolerant vegetation photosynthetic activity (e.g. Fig. 3a). Therefore, in the drier north region of the basalt aquifer, a surface indicator of both fresh and saline groundwater discharge areas is the relatively low seasonal variability of the vegetation photosynthetic activity. The inter-annual variability of the vegetation activity can also contain useful information to map groundwater discharge areas. The intensive agricultural activities that characterise most of the region such as harvesting, ploughing, grazing, and culture rotation, affect the vegetation activity. However, groundwater discharge areas often have low agricultural yield, are difficult to access or require drainage, and are generally not farmed or are farmed to a lesser degree than other areas.

Areas in the landscape where groundwater discharge to the surface is likely to occur include topographic depressions and at the break of slope in lower areas of the terrain, which commonly results in discharge to wetlands and rivers. Groundwater discharge via evaporation and transpiration are also likely to increase within topographic depressions and at break-of-slope areas due to general correlations with shallower depth to water tables. For example, in semi-arid regions, evaporative pans within topographic depressions actively evaporate moisture from the subsurface (Thorburn et al. 1992).

Potential indicators of groundwater discharge include a shallow water table, the lower temporal variability of the vegetation activity, terrain indicators such as topographic depressions and break of slope, and groundwater flow direction towards surface water bodies (rivers, wetlands, and the ocean).

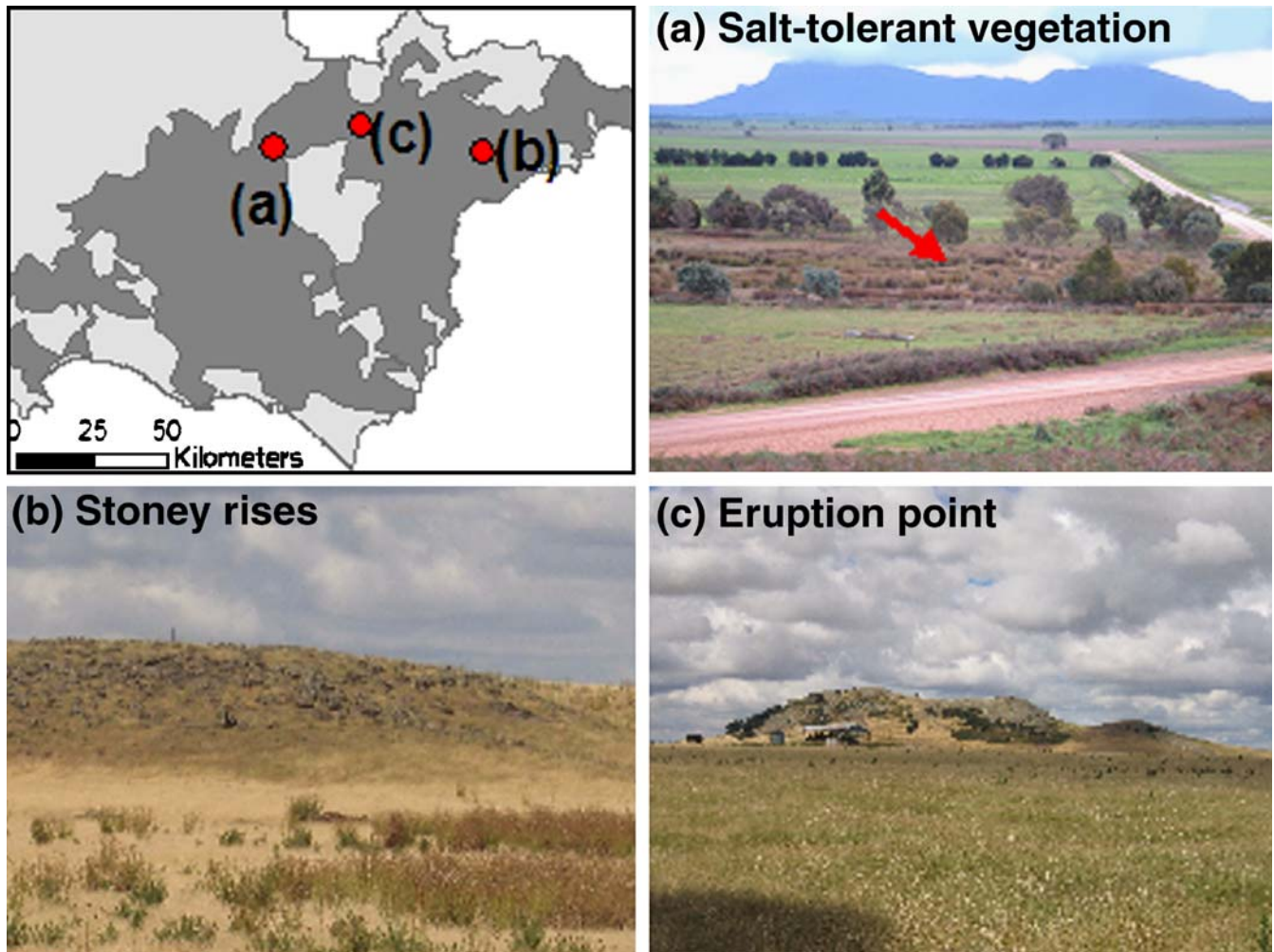


Fig. 3 Examples of surface indicators for discharge areas: **a** salt-tolerant vegetation, and recharge areas: **b** stoney rises (basalt lava with irregular surface morphology) and **c** eruption point. Note that the surface extent of the stoney rises can be several square kilometres, and are mapped in detail in the following sections, whereas the eruption points cover much smaller areas

Recharge processes

All locations where groundwater is not discharging are potential recharge areas. Factors that can affect the spatial distribution of relative recharge fluxes, or the location of preferential recharge areas, include increased rainfall and increased infiltration capacity of the soil. Increased rainfall in the southern region of the basalt aquifer (Fig. 2) may affect relative recharge rates across the region. However, within this region, a major control on the location of preferential recharge areas is the hydraulic properties of the soil profile and unsaturated zone.

Within the basalt aquifer, increased shallow-zone infiltration rates are associated with areas of thin soil/clay profiles such as the profiles of the less-weathered basalt flows, stoney rises, and eruption points (Fig. 3b and c). Previous investigations within the study area have highlighted that the less-weathered basalt is typically the youngest of the basalt flows (<0.5 Ma), which have thinner and more rocky soil profiles compared with the older basalt flows (~2–4 Ma) (Joyce 1999; Bennetts et al. 2003). An example of the relatively undeveloped weathered profiles of the basalt includes the stoney rises (an

example is shown in Fig. 3b). Stoney rises are areas of irregular basalt boulders at the surface, providing effective conduits for recharge. In comparison, the more weathered basalt has thick (5–15 m) kaolinitic regolith profiles (Bennetts et al. 2003), thereby reducing the potential recharge flux. Eruption points are associated with all of the basalt flows, form locally elevated areas (Fig. 3c), and, in general, have poorly developed soil/clay profiles (Bennetts and Webb 2004). Therefore, within the study area, indicators of preferential recharge areas include less-weathered basalt flows, stoney rises, and eruption points.

Potential recharge areas, outside of preferential recharge areas, will have a relatively lower flux of water reaching the water table due to the compounded effects of lower infiltration rates and increased evapotranspiration of the recharging water.

Methods and data

Methodology

The method used in this study for mapping groundwater recharge and discharge areas incorporated GIS and remote-

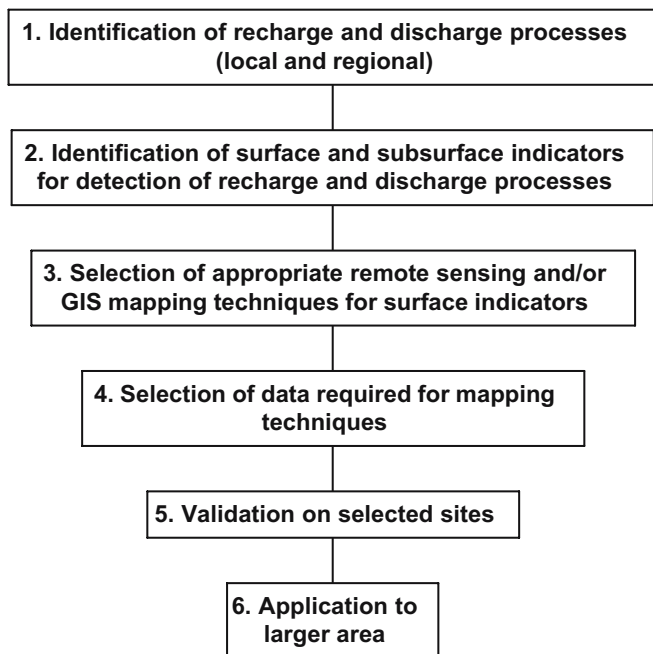


Fig. 4 Outline of the methodology

sensing mapping techniques to link catchment features with groundwater recharge and discharge processes. As outlined in Fig. 4, the first two steps involved using knowledge of the local hydrogeology to identify a series of surface/subsurface indicators that best show recharge and discharge processes. Steps three and four involved selecting adequate remote sensing and GIS techniques, as well as necessary datasets. Lastly, the results of mapping the indicators were validated on test sites, and if successful, the mapping of these surface indicators was then applied to the entire basalt aquifer. The surface/subsurface indicators, associated datasets, and validation techniques used to map groundwater discharge and preferential recharge areas for the basalt aquifer are outline in detail below, and are summarised in Fig. 5a and b.

Mapping discharge and preferential recharge areas relied on a variety of GIS (DEM terrain analysis; grid interpolation) and remote sensing (time analysis of photosynthetic vegetation activity, image interpretation, simple threshold, and airborne radiometrics) techniques. The GIS and remote-sensing software used in this study were ArcGIS 9.0 (ESRI 2005) and ENVI 4.2 (ITT 2005), respectively. Remote sensing and GIS techniques required multi-source and multi-scale datasets including groundwater monitoring data, airborne (radiometrics and aerial photos), satellite (Landsat), and GIS (soil map, DEM, groundwater EC, flow, and depth to the water table) maps. The spatial resolution and sources of these datasets are outlined in Table 1.

Indicators of groundwater discharge areas

Low variability of the vegetation activity

The rationale for mapping discharge areas using low variability of the vegetation photosynthetic activity, as

outlined above (see section [Discharge processes](#)), is that in the drier north, both fresh and saline discharge areas exhibit a constant photosynthetic activity when compared with productive agricultural areas in the landscape over seasonal and yearly time periods. A time series of nine Landsat (TM and ETM+) data, from 1989 to 2003, were used to map temporal changes of the vegetation photosynthetic activity across the northern region of the aquifer. First, relative radiometric normalisation was applied using pseudoinvariant targets to correct for inter-scenes radiometric variability relating to change in the instrument or the atmosphere rather than change on the ground. The NDVI was then calculated for each image Eq. (1). Then, the variability of the vegetation activity was obtained by calculating the standard deviation of the NDVI (SDVI) on a pixel by pixel basis Eq. (2). The map generated shows standard deviation values of the vegetation index for every pixel, and represents the temporal variability of the vegetation photosynthetic activity throughout the years.

$$\text{NDVI} = (\text{NIR} - \text{red}) / (\text{NIR} + \text{red}) \quad (1)$$

$$\text{SDVI} = \sqrt{\frac{1}{n} \sum_{i=1}^n (\text{NDVI}_i - \text{NDVI}_{\text{mean}})^2} \quad (2)$$

Where n is the number of scenes and $\text{NDVI}_{\text{mean}}$ is the mean NDVI for each pixel.

Regions of lowest variability of the photosynthetic activity were detected using a simple threshold technique on the SDVI image. This mapping was applied only for the dryer northern region, where rainfall is the limiting factor of vegetation growth in the summer. For this northern region, the aridity index has values $0.50 < \text{AI} < 0.65$ representing sub-humid conditions.

Along with groundwater discharge areas, roads, urban areas, and forests also exhibit low SDVI. These areas were masked from the analysis. Ongoing research work, to be submitted for publication elsewhere, is currently looking at improving the validation and application of this SDVI technique to map discharge areas (see also section [Discussion](#)).

Topographic depressions and break of slope

As demonstrated in many studies (Moore et al. 1991; Vieux 1995; Wilson and Gallant 2000), topographic indices interpreted alongside other datasets may provide a useful indicator of hydrological processes. Two indices were generated from a DEM of the region to indicate potential groundwater discharge in topographic depressions and at break of slope across the whole basalt aquifer. In both techniques, the indicator will only represent groundwater discharge areas if the depth to the water table is shallow.

To indicate topographic depressions, a topographic wetness index was derived from the DEM. The modified wetness index (w) has been used to describe areas of

surface saturation in the landscape and was calculated using the following equation (Moore et al. 1991),

$$w = \ln \left(\frac{1}{\tan \beta} \right), \quad (3)$$

where β is the slope gradient (in degrees). The wetness index was used to identify potential zones of saturation at the base of concave slopes (a decrease in the β ; Moore et al. 1991). A simple threshold technique (>10) was used on the wetness index to map topographic depressions and the areas of potential groundwater discharge.

To map the break of slope of the terrain, the profile curvature GIS function was used on the DEM. Profile curvature is the curvature of the terrain in the direction of the slope. The curvature of a surface is calculated on a cell-by-cell basis. The output of this curvature function is the second derivative of the surface (i.e. the slope of the slope) and was used in this study to indicate the break of slope. A positive profile indicates that the surface is concave at that cell. A value of zero indicates that the slope of the terrain is constant. A simple threshold technique (>0.01) was used to map the highest profile curvature values from the DEM and detect the breaks of slope.

Groundwater flow lines, permanent water bodies, and shallow water table

Groundwater data from the Victorian Department of Sustainability and Environment Groundwater Database, and Centre for Land Protection Research Groundwater Database were used to generate a groundwater flow-direction map for the basalt aquifer. Hydraulic head data were collated from bores screened in the basalt aquifers at <35 m depth. The locations of the bores used for this study are presented in Fig. 1a. Hydraulic head data were interpolated using the inverse weighted distance method (7 neighbours) in ArcMap. The resulting grid was used to generate groundwater potentiometric contours. The convergence of groundwater flow directions was used to indicate regional areas of groundwater discharge. These groundwater datasets were also used with the DEM in the GIS to produce a map of the depth to the water table. A map of depth to the water table <5 m was used as an approximate indicator of areas where the groundwater is increasingly evaporated and potentially discharging to the surface. The permanent wetlands GIS data were selected from the Victorian Departments of Primary Industries and Sustainability and Environment Corporate Geospatial Data Library (Table 1).

Indicators of preferential recharge areas

Volcanic features (eruption points and stoney rises)

As outlined previously, volcanic eruption points and areas of stoney rises can have relatively high infiltration rates. Areas of stoney rises were identified using visual image interpretation from Landsat ETM+ true colour composi-

tion images and aerial photographs. The locations of eruption points were detected as topographically high features in the DEM and confirmed using photo-interpretation of aerial photographs. The eruption locations were cross-validated with information from on-going geological mapping (Ray Cas, Monash University, Australia, unpublished data, 2005; Matthias Raiber, La Trobe University, Australia, unpublished data, 2006). The location of some stoney rises and eruption points were also ground-truthed.

Less-weathered basalt

In this study, less-weathered basalts were identified using a simple threshold technique to delineate the regions of high potassium (K) and low thorium (Th) in the airborne radiometric (gamma-ray spectrometry) data. Previous investigations have used variations in the K, uranium (U) or Th in airborne radiometric images to map the extent of different aquifers (Bierwirth and Welsh 2000). This technique was also used by Joyce (1999) and Bennetts et al. (2003) to distinguish less-weathered basalt from basalt overlain by thicker clay/soil profiles.

Soil infiltration properties

The soil drainage map, obtained from the Victorian Departments of Primary Industries and Sustainability and Environment Corporate Geospatial Data Library (Table 1), was also included as a general indicator of soil infiltration capacity. The soil drainage relates to the average wetness or dryness of a soil due to changes in soil texture, structure, slope of the land, and absence or presence of a high water table. Soils that are well to rapidly drained (dry for long periods) are likely to have a high-infiltration capacity and were, therefore, considered as an indicator of preferential recharge areas.

Validation datasets

For the selected test sites (Fig. 1a), the discharge indicators outlined above were compared with on-ground field data such as soil salinity, depth to groundwater, and vertical hydraulic gradients. A map of salinity-affected soil and salt-tolerant vegetation was constructed independently of this study by Munro (2000; Table 1).

On-ground data were also used to validate the techniques used to map preferential recharge areas, and include potentiometric contours, vertical hydraulic gradients, and groundwater EC values. Low EC values for shallow groundwater can indicate areas of preferential recharge, as there is increased freshwater input and less time for either evapotranspiration or mineral dissolution processes to result in increased solute concentrations. Subsequent increases in groundwater EC values with flow down-gradient from preferential recharge areas primarily results from evapotranspiration of infiltrating rainfall and shallow groundwater (Bennetts et al. 2006).

Table 1 Resolution and datasets used for the different indicators

Indicator	Spatial resolution of indicator (m)	Data type	Input data	Spatial resolution of input data (m)	Data processing
Discharge					
SDVI	30	Raster	7 Landsat TM data : 15/01/1998, 4/02/1995, 18/02/1993, 11/10/1991, 12/01/1991, 08/12/1989, 08/09/1994 ^a and 2 Landsat ETM+ data : 21/01/2003 and 10/01/2002 ^a	30	Standard deviation of NDVI
Topographic depression	100	Raster	DEM ^b	20	Wetness index
Break of slope	50	Raster	DEM ^b	20	Profile curvature
Depth to water table	250	Raster	DEM ^b and Groundwater monitoring data ^c	20; 2,661 bores	DEM-hydraulic head
Groundwater flowlines		Vector polyline	Groundwater monitoring data ^c	2,661 bores	Interpolation (inverse distance weight and 7 neighbours) and contouring of hydraulic head data ^h
Permanent wetlands		Vector polygon	Wetland inventory mapping ^b		
Recharge					
Stoney rises		Vector polygon	Landsat ETM+ true colour composition images ^a and aerial photographs ^d	30; 1.25	Visual interpretation and ground truthing
Eruption points		Vector point	DEM ^b and aerial photographs ^d	20; 1.25	Visual interpretation and ground truthing
Less-weathered basalt		Vector polygon	Airborne radiometric data ^b	50	Threshold technique on K and Th bands ^h
Soil infiltration		Vector polygon	Soil drainage property mapping ^b		
Additional data					
Land-use map	30	Raster	2002 land use mapping ^e	30	^h
Aridity index	10,000	Raster	Gridded rainfall and potential evapotranspiration ^f	2,500; 10,000	Rainfall/ potential evapotranspiration
Monthly rainfall		Vector point	Average monthly rainfall station data ^f	15 stations	
Groundwater EC	250	Raster	Groundwater monitoring data ^c	2,870 bores	Interpolation (inverse distance weight and 7 neighbours) of groundwater EC data ^h
Salinity-affected soil and vegetation map		Vector polygon	Saline sites mapped where two or more of the local salt-tolerant plant species were present ^g		

Data sources:

^aUS Geological Survey, Australian Greenhouse Office, and Australian Centre for Remote Sensing

^bVictorian Departments of Primary Industries and Sustainability and Environment Corporate Geospatial Data Library

^cVictorian Department of Sustainability and Environment Groundwater Database, and Centre for Land Protection Research Groundwater Database (data from bores screened <35 m depth)

^dGlennelg-Hopkins Catchment Management Authority

^eIerodiaconou et al. (2005)

^fBureau of Meteorology

^gMunro (2000)

^hData already processed by the reference

Results

Indicators of groundwater discharge areas

The systematic mapping of discharge areas involved identifying areas of stable vegetation activity, topographic depressions, break of slope, shallow depth to the water table, groundwater flow directions, and permanent surface-water bodies.

Low variability of the vegetation activity

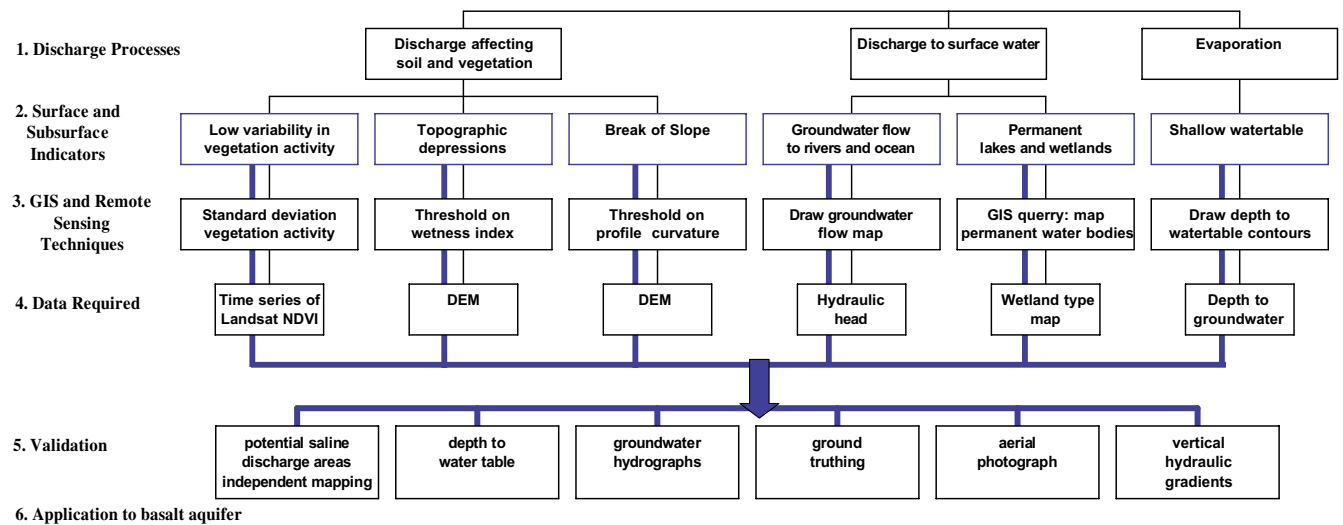
The standard deviation for the vegetation index (SDVI) was mapped for the dryer region of the basalt aquifer, and ranges in values from 0.07 to 0.47 (Table 2). As outlined previously (see section [Methodology](#)), relatively stable photosynthetic activity of vegetation indicates potential groundwater discharge areas. A SDVI threshold value of

0.20 was used where values <0.20 indicate potential discharge areas.

As a first step in validating the use of SDVI, values for saline soil areas mapped by Munro (2000) are compared with the surrounding agricultural land. The results indicate a lower mean SDVI of 0.20 for the saline soil areas, compared with 0.25 for the surrounding agricultural zones (Table 2). Figure 6a shows the histograms for the SDVI values inside saline soil areas and for agricultural areas. In saline discharge areas, 52% of the SDVI values are below the 0.20 threshold, compared with only 5% of SDVI values for agricultural areas <0.20 .

A test site to assess groundwater discharge mapping was selected in the northern region of the aquifer (Fig. 1a). In this area, the SDVI results are presented in detail and on-ground data were also used to validate application of

(a)



(b)

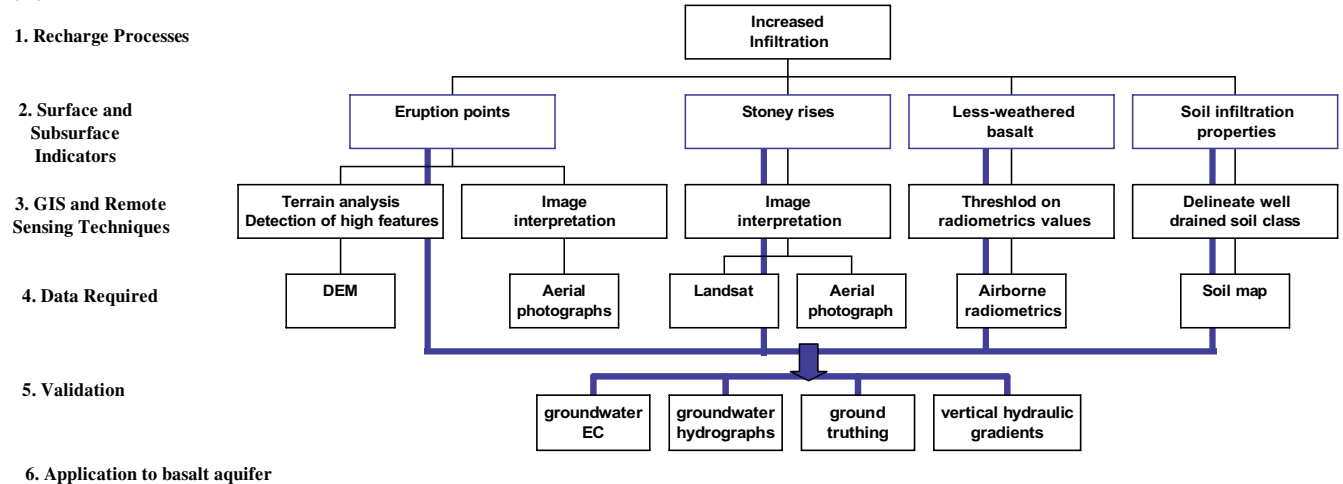


Fig. 5 a Method for mapping discharge areas in the study area. Application of the standard deviation of the vegetation index (SDVI) to north region; all other indicators applied to the whole basalt aquifer. DEM digital elevation model; NDVI normalized difference vegetation index. b Method for mapping preferential recharge areas in the study area

the indicator. Four examples of potential discharge areas are outlined in red (Fig. 7b). As shown in aerial photograph (Fig. 7b), some of these discharge sites also include areas of inundation. In Fig. 7a, examples of four paddocks are also shown. The mean SDVI inside the discharge areas is lower (0.20) compared with the paddocks (0.27). These values indicate a relatively stable vegetation activity in the groundwater discharge areas compared with agriculturally active areas. On-ground data support the results of these discharge areas mapped using SDVI. The depth to groundwater is <5 m, groundwater potential contours indicate a general convergence of flow lines toward this area, and nested bores indicate an upward hydraulic gradient (averages -0.004 and -0.002 ; Fig. 8a). Additionally, the average groundwater EC is relatively high proximal to the discharge areas (Fig. 8a).

Topographic depressions

The wetness index was mapped for the entire basalt aquifer, and ranges in values from 5.3 to 20.1. Areas where the wetness index is high (threshold: >10) indicates regions of topographic depressions, and, therefore, potential groundwater discharge areas. These areas are found across the entire aquifer covering $\sim 2,000$ km², which is 17% of the basalt aquifer.

The results of statistical analysis for the northern region of the basalt aquifer indicate a slightly higher mean value of 9.9 for saline soil areas (Munro 2000), compared with 9.3 for surrounding agricultural areas (Table 2). Additionally, histogram results shown in Fig. 6b indicate that approximately 42% of the wetness index values for the saline soil areas are >10 , compared with 16% of the wetness index values >10 for surrounding agricultural zones. These results suggest that for the basalt aquifer, the wetness index can be a useful indicator of saline groundwater discharge in agricultural regions.

The results of the wetness index mapping are presented in Fig. 7c for the same test site presented for the SDVI results in Fig. 7a. In this example, the topographic depressions, represented by high wetness index values (>10), generally correlate to the discharge areas indicated by the SDVI (Fig. 7d), and, therefore, shallow depth to

water table, upward hydraulic gradients, and increased groundwater EC (Fig. 8a).

Break of slope

The profile curvature values for the basalt aquifer region range from -0.62 to 0.49 . Profile curvature values greater than 0.01 , were considered to highlight break-of-slope areas as potential groundwater discharge areas. Break-of-slope areas were mapped across all of the basalt aquifer, with a total surface area of $\sim 1,800$ km² (16% of the basalt aquifer).

For the northern region of the basalt aquifer, the profile curvature ranges in values from -0.07 to 0.15 for saline soil zones, and from -0.62 to 0.46 for surrounding agricultural areas (Table 2). The histograms of the profile curvature values for the two regions show a similar distribution (Fig. 6c). Approximately 11% of the profile curvature values for the saline soil areas are above the 0.01 threshold, which is similar to the $\sim 9\%$ of values in agricultural areas. Thus, in comparison to the SDVI and topographic depression indicators, the results shown in Fig. 6 suggest that the break-of-slope indicator is less successful in detecting potential saline discharge areas from surrounding agricultural areas.

In the test site, the results of mapping show that the break-of-slope areas surround some of the saline soil areas (Fig. 7c). Thus, a break of slope may be useful to indirectly identify potential groundwater discharge areas. However, also evident from the test site shown in Fig. 7c are the abundant break-of-slope areas in the northeast, where there is little evidence of groundwater discharge.

Groundwater flow lines, permanent water bodies, and shallow water table

At the regional scale of the study area, the general flow lines indicate regional groundwater discharge to the major rivers and the ocean (Fig. 9). At a more localised scale, the potentiometric contours within the selected test site indicate a convergence of groundwater flow towards the southwest, where the SDVI and wetness index also indicate groundwater discharge (Fig. 7d).

Permanent wetlands were also mapped as potential groundwater discharge areas in Fig. 9. For these shallow surface water bodies, groundwater is an important component sustaining water levels during dry periods. Within the study region, there are 485 permanent wetlands that cover a total of 0.8% (88 km²) of the area overlying the basalt aquifer. Most of these wetlands are located in the northern region of the basalt aquifer.

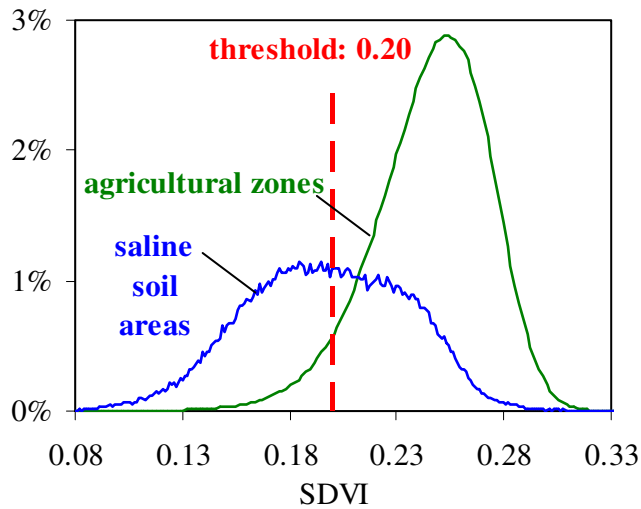
The depth to the water table is also shown in Fig. 9, and areas where the depth is <5 m indicate regions where there is increased potential for groundwater discharge via evaporation. The rate of groundwater evaporation will vary greatly across any catchment depending on factors such as climate, soil properties, and depth to the water table. Therefore, this map only highlights potential areas of relatively increased rates of groundwater evaporation

Table 2 Vegetation activity and terrain indices statistics for the northern region

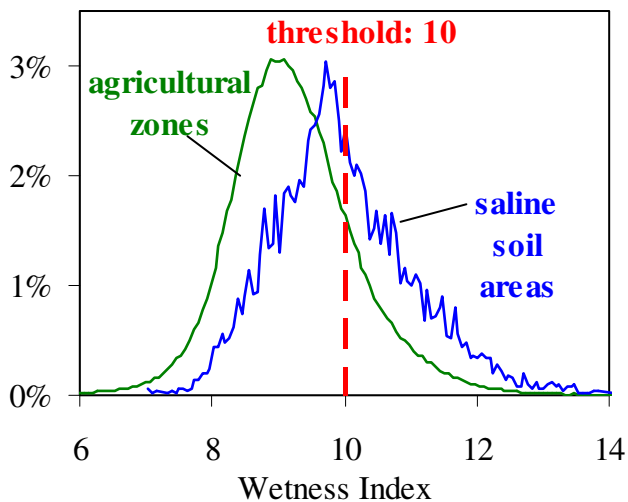
	Minimum	Maximum	Mean	Standard deviation
SDVI				
Agricultural zones	0.07	0.47	0.25	0.03
Saline soil areas ^a	0.07	0.36	0.20	0.04
Break of slope				
Agricultural zones	-0.62	0.46	0.00	0.02
Saline soil areas ^a	-0.07	0.15	0.00	0.01
Wetness index				
Agricultural zones	5.3	16.7	9.3	1.0
Saline soil areas ^a	7.0	14.8	9.9	1.1

^a Areas mapped by identifying salinity-affected soil and salt-tolerant vegetation (Munro 2000)

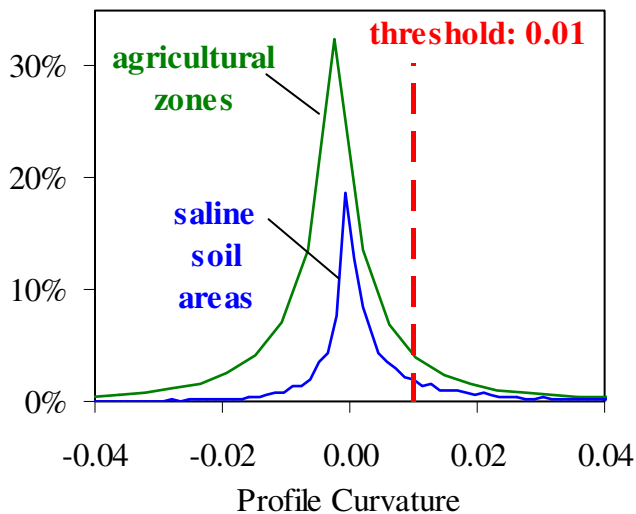
(a) Vegetation Activity (SDVI)



(b) Topographic Depression



(c) Break of Slope



◀ **Fig. 6** Distribution of values for the **a** vegetation activity using the SDVI, **b** topographic depressions using the wetness index, and **c** region of the study area. The values are presented for two categories: agricultural zones and saline soil areas. The saline soil areas have been mapped by identifying salinity-affected soil and salt-tolerant vegetation are as via aerial photo graphs and field surveys (Munro 2000)

compared with surrounding areas. Throughout the basalt aquifer, 14% of the region has depth to water <5 m, totalling ~1,650 km². The shallow depth to water table (<5 m) is found in both fresh and saline groundwater areas.

Indicators of preferential recharge areas

Volcanic features, less-weathered basalt, and soil infiltration properties were used to map areas of relatively high infiltration potential, which are identified as areas of preferential recharge.

Volcanic features (eruption points and stoney rises)

The results of mapping stoney rises for the basalt aquifer, and the location of eruption points are presented in Fig. 10a. The stoney rises areas are distributed along the eastern margin and in the south of the basalt aquifer, and cover 976 km², or ~8% of the surface area. An example of these areas in aerial photograph is shown in Fig. 10b.

A test site presented in Fig. 8b highlights the relatively high hydraulic heads within the stoney rises area. Hydraulic head data from nested bores located in this preferential recharge area (Fig. 8b) show a greater fluctuation in the shallow zone (2–8 m) compared with increasingly attenuated responses to rainfall with increasing depth (18–24 m and 46–49 m). There is also a downward vertical hydraulic gradient (average 0.053, Fig. 8b). In comparison, the groundwater hydrograph for a shallow (2–23 m) bore located outside of the preferential recharge area shows a relatively attenuated response to rainfall (Fig. 8b). The attenuated response may be due to a combination of lower infiltration rates, variations in specific yield, and a larger unsaturated zone (~13 m) compared with the preferential recharge area (<5 m).

The test site presented in Fig. 8b also highlights the relatively low groundwater EC within the stoney rises area. Figure 11 illustrates the change in groundwater EC values with distance from the stoney rise area (from the test site). Results indicate that 95% of the maximum change in average groundwater EC has occurred within 4–6 km from the stoney rise area. Figure 10a shows a general correlation between the stoney rises areas and relatively low groundwater EC values across the whole aquifer. For the southern and northern regions of the aquifer, 81 and 77%, respectively, of the groundwater EC measurements within the stoney rises areas are lower than the average groundwater EC values in the surrounding 5-km buffer zone. Comparisons are undertaken separately for the northern and southern regions, because merging

comparisons of groundwater EC values is complicated by the spatial variability in climate (Fig. 2). Histogram results for the southern region are presented in Fig. 12a. The greater frequency of lower groundwater EC values from bores located within stony rises areas, compared with the surrounding 5-km buffer zone, indicate relatively higher recharge rates of rainfall.

Less-weathered basalt

The results of mapping the location of less-weathered basalt, using the airborne radiometric data, are presented in Fig. 10c. The distribution of these areas mostly matches that of the stony rises (Fig. 10d). Also similar to the stony rise areas within the southern and northern regions, 81 and 76%, respectively, of the groundwater EC measurements within the less-weathered basalt areas have lower than the average groundwater EC values from the surrounding 5 km buffer zone (Fig. 12b). Compared with

the stony rises area, an additional 1,000 km² of less-weathered basalt, predominantly in the south, was detected using airborne radiometric data (Fig. 10d). As in stony rises areas, lower groundwater EC values and increased responses to rainfall in water-table fluctuations are also observed in the test site for these areas of less-weathered basalt.

Soil infiltration properties

Mapped areas of well to rapidly drained soils mostly correlate to the distribution of stony rises, eruption points and less-weathered basalt (Fig. 10d). These areas cover 1,655 km², which is 14% of the basalt aquifer surface. There are two large areas where the increased soil infiltration property does not correlate to the other indicators. The distribution of groundwater EC values below the buffer zone average within the southern and northern regions (77 and 83%, respectively) is similar to

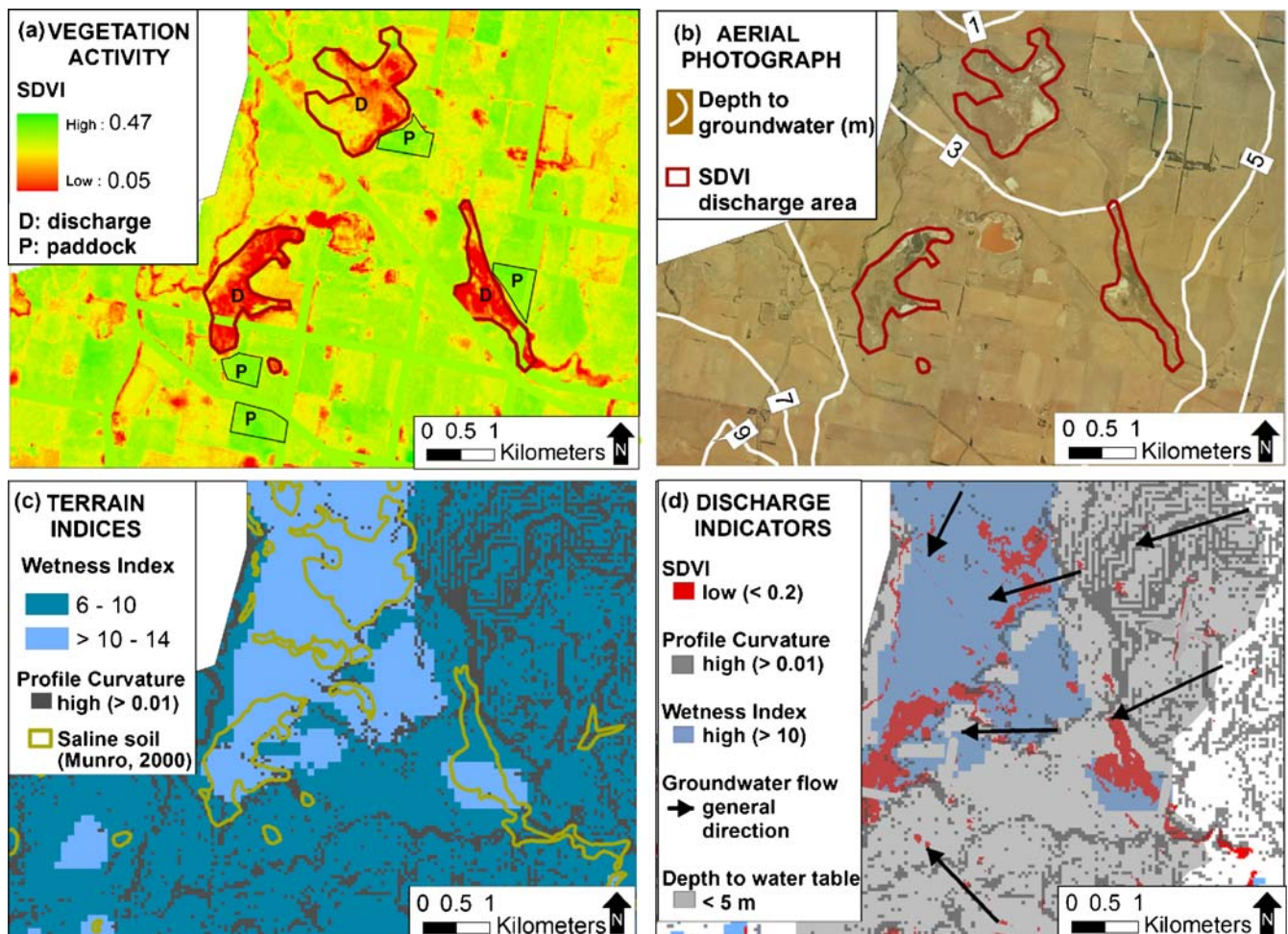


Fig. 7 Test site with mapped discharge indicators. The test site is located in the northeast area of the study region (location shown in 1a). **a** The SDVI for discharge areas compared with agricultural regions (paddocks). The values for roads have been masked. **b** The aerial photograph highlights land use for the different regions analysed, and shallow depth to water contours indicates that it is a potential discharge area. **c** Terrain indices mapped: wetness index to highlight topographic depressions, and profile curvature to map break-of-slope areas. Saline soil areas mapped by Munro (2000) are also shown. **d** All discharge indicators: relatively low SDVI, positive profile curvature, high wetness index, groundwater flow lines and shallow depth to water table

the stoney rises and less-weathered basalt indicators (Fig. 12c).

Application to the whole aquifer

The final map of recharge and discharge areas for the basalt aquifer is presented in Fig. 13. A simple GIS exclusion was used to present all regions that are not discharge areas as potential recharge areas. Within the potential recharge areas, preferential recharge areas were mapped.

The final map includes most indicators listed above; however, the break-of-slope indicator was not used as it gave poor results in the test sites. Additionally, groundwater flow lines indicated regional flow to major rivers

and the ocean; therefore, these discharge sites are mapped instead of the groundwater flow lines.

Verification of the final mapping for the whole aquifer involved comparison with predicted recharge/discharge process from vertical hydraulic gradients of nested bores and depth to water table. Average vertical hydraulic gradients were calculated for 20 sites of nested bores, typically with ~10 years of head monitoring data (Table 3). At each of the 20 sites, a predicted process was assigned, where discharge was estimated if an upward gradient and depth to water table <5 m was observed. The locations of the 20 sites for analysis are shown in Fig. 13, and results are presented in Table 3. Predicted recharge/discharge processes for 17 of the sites were in agreement with the mapped indicators of recharge/discharge areas.

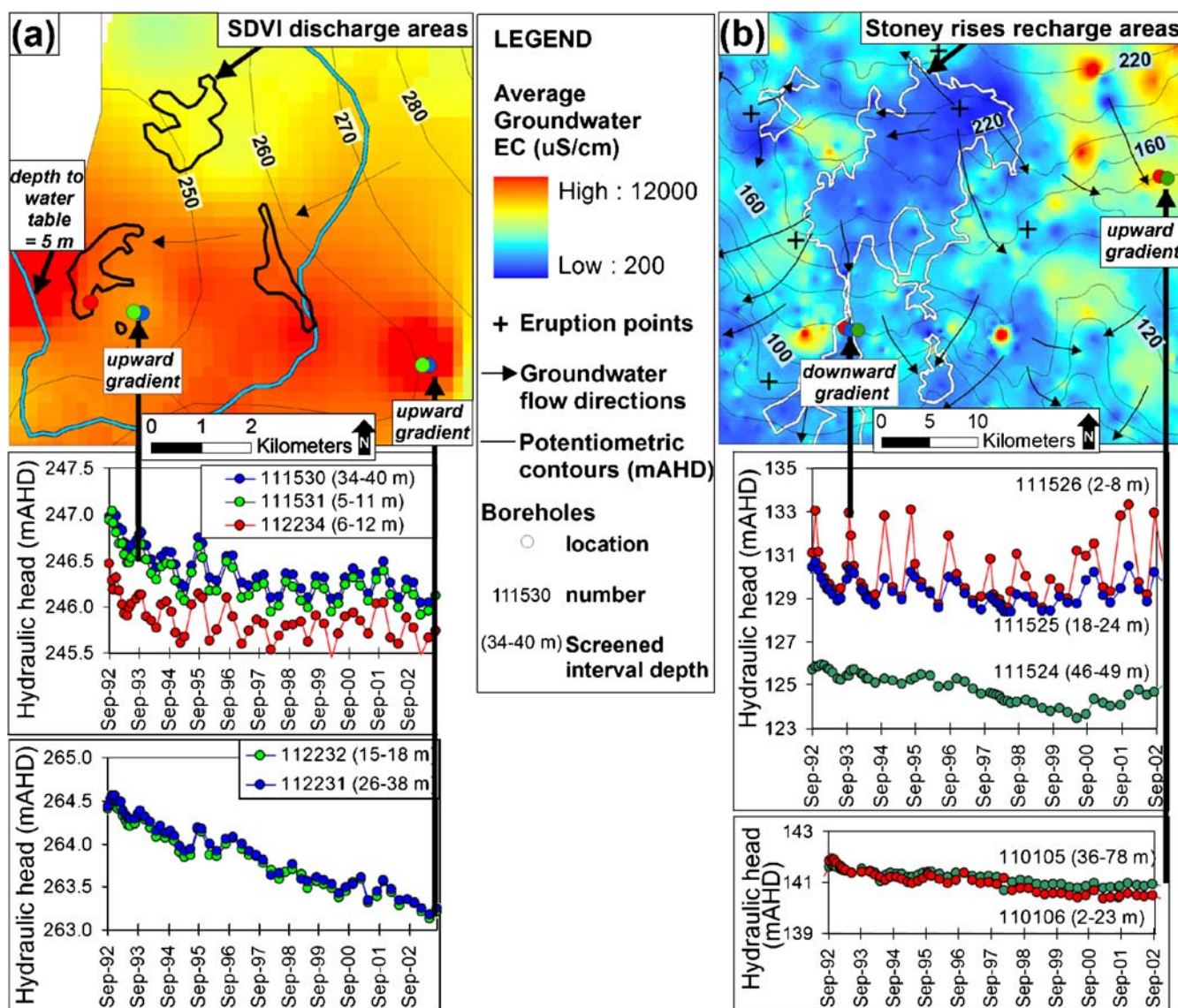


Fig. 8 Assessment of the surface indicators in selected test sites. Average groundwater electrical conductivity (EC) and hydrograph results are compared with indicators for **a** groundwater discharge areas (thick black lines), and **b** preferential recharge areas (white lines). Hydraulic gradients are also shown (upward, downward). The location of the stoney rises recharge areas in **b** is shown in Fig. 1a. Hydraulic head in metres above Australian Height Datum (mAHd)

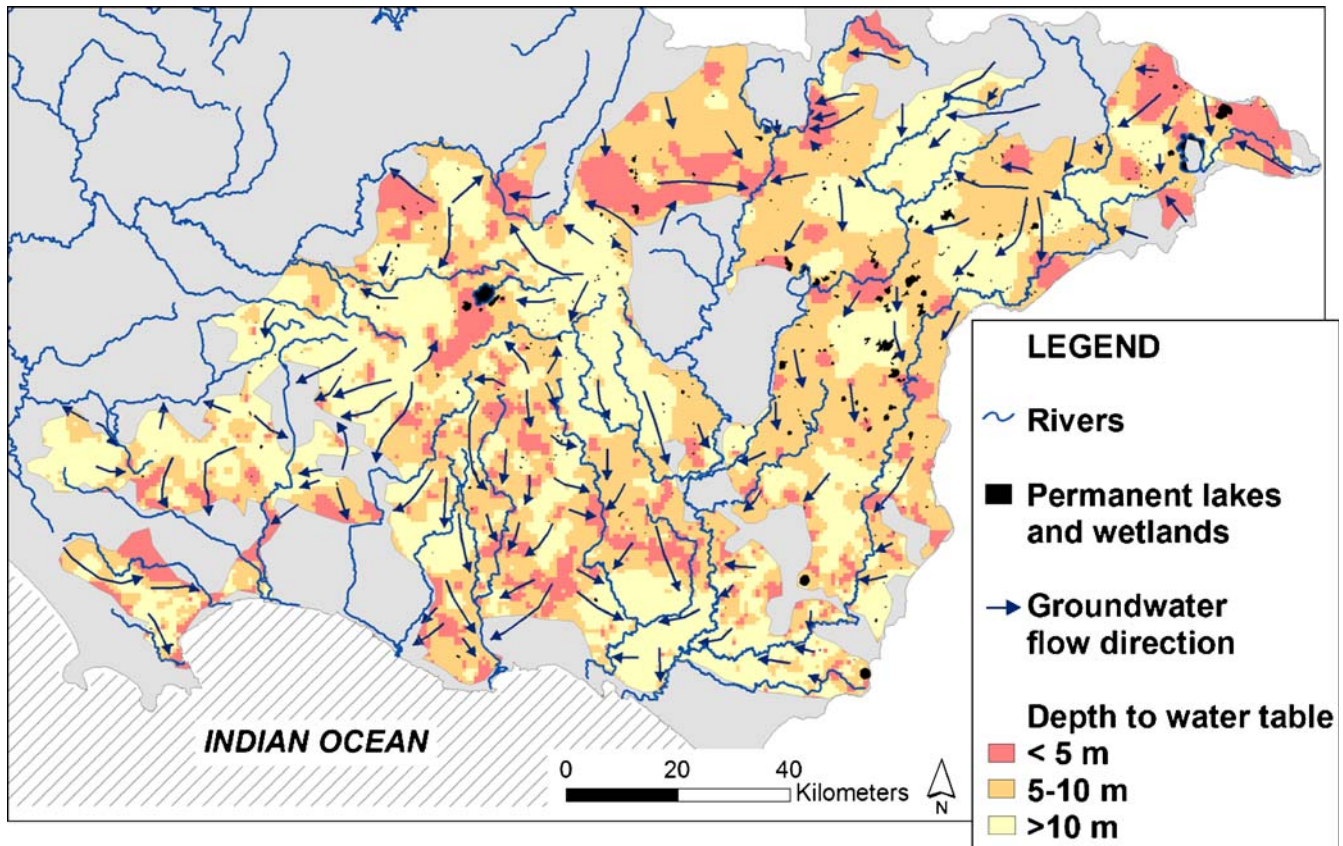


Fig. 9 General groundwater flow map indicating groundwater discharge to major rivers and the ocean, permanent wetlands, and depth to the water table

Discussion

In this study, the mapping enabled spatial definition of preferential recharge, and potential discharge and recharge zones at a fine resolution across the $\sim 11,500 \text{ km}^2$ aquifer. Traditional mapping of recharge and discharge areas has often relied on bore data (especially potentiometric surfaces and depth to groundwater data). However, here it would not have been possible to detect most recharge and discharge areas by just using bore data due to their lower spatial density. Preferential recharge areas are not just elevated regions in the topography, and as discussed below, discharge areas do not encompass whole areas of topographic lows.

Discharge

The SDVI indicator can be used to detect areas where groundwater either supports or inhibits vegetation activity. The technique has the potential to highlight both fresh and saline groundwater discharge, and regions where vegetation is groundwater dependent. The technique requires development; however, preliminary ground-truthing shows good results in the drier, north of the basalt aquifer. The

technique may be more limited in the southern region where rainfall is higher (Fig. 2). The SDVI data should also cover changes in long-term climatic variations. For example, drought conditions have affected groundwater systems in southeastern Australia since the mid-1990s, resulting in decreased vegetation activity for paddocks and discharge areas. The timeframe for change detection should, therefore, be taken into consideration when using the SDVI technique. The SDVI was derived from a number of images so it is dependent upon the temporal scheme of sampling (Table 1). Ongoing research work is looking at improving the SDVI indicator by selecting satellite data with a higher frequency over a shorter period.

Of the topographic indices used in this study, the topographic depression is a better indicator of groundwater discharge areas compared with the break-of-slope indicator (Fig. 6b and c), and is, therefore, used for the final map in Fig. 13. The surface area of the mapped topographic depressions is greater than that of the SDVI (Fig. 7d). This may be due to the SDVI reflecting more localised discharge processes occurring within the larger topographic depressions. Future work in the region should reassess the topography indicators with a higher accuracy DEM.

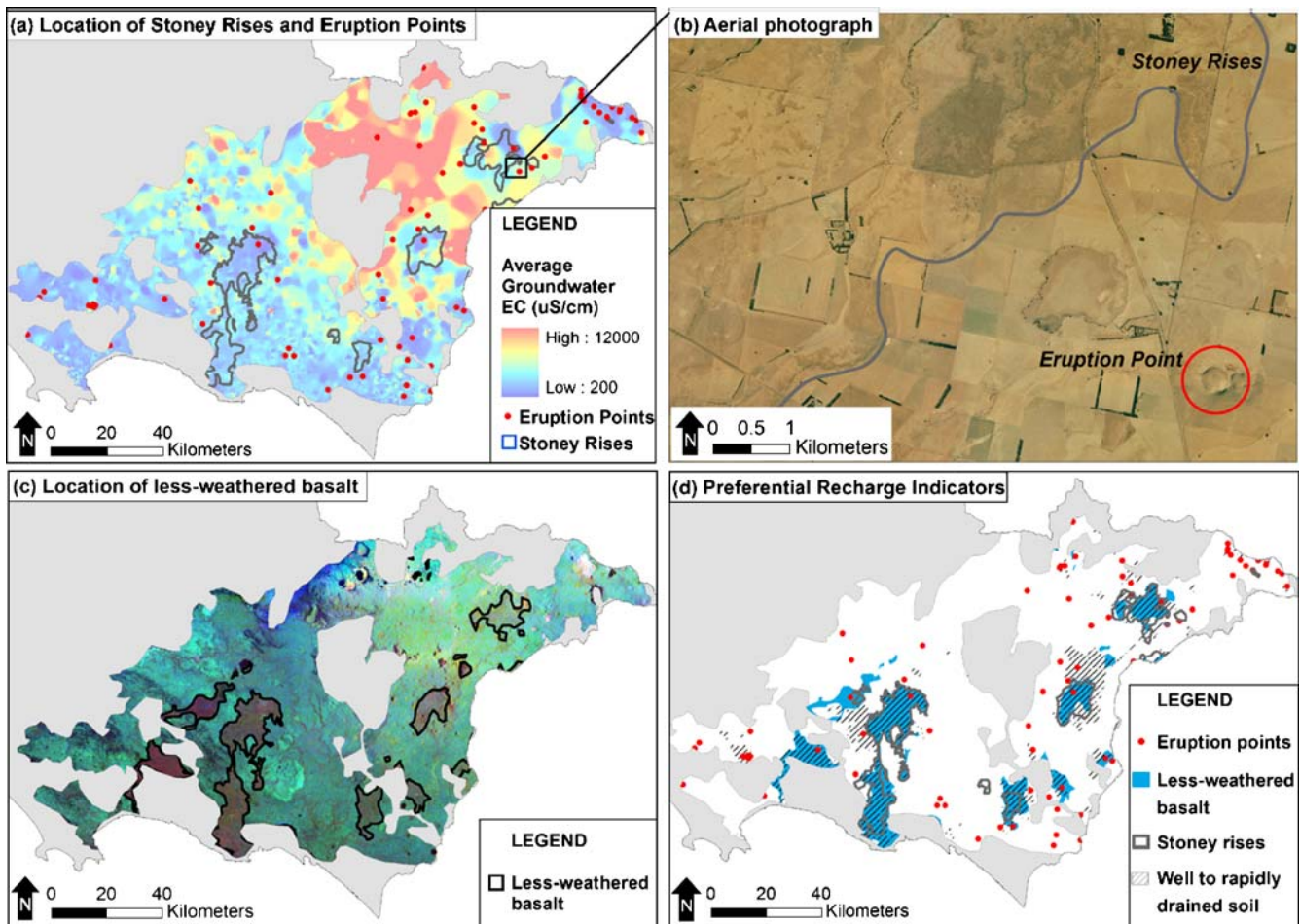


Fig. 10 Indicators used to map preferential recharge areas across the basalt aquifer includes **a** the location of stoney rises and eruption points, which generally correlates to low average groundwater EC values. **b** An example of the stoney rises and eruption point in aerial photograph. **c** Mapping of less-weathered basalt using airborne radiometric data, where red represents potassium (K); blue represents uranium (U); green thorium (Th). **d** All indicators used to map preferential recharge areas, including the volcanic features and soil in filtration properties

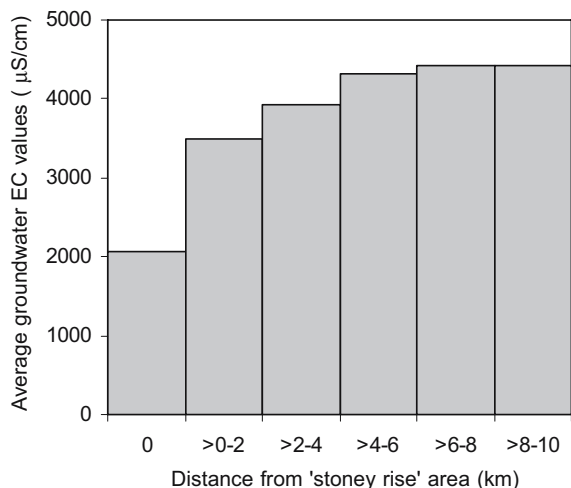
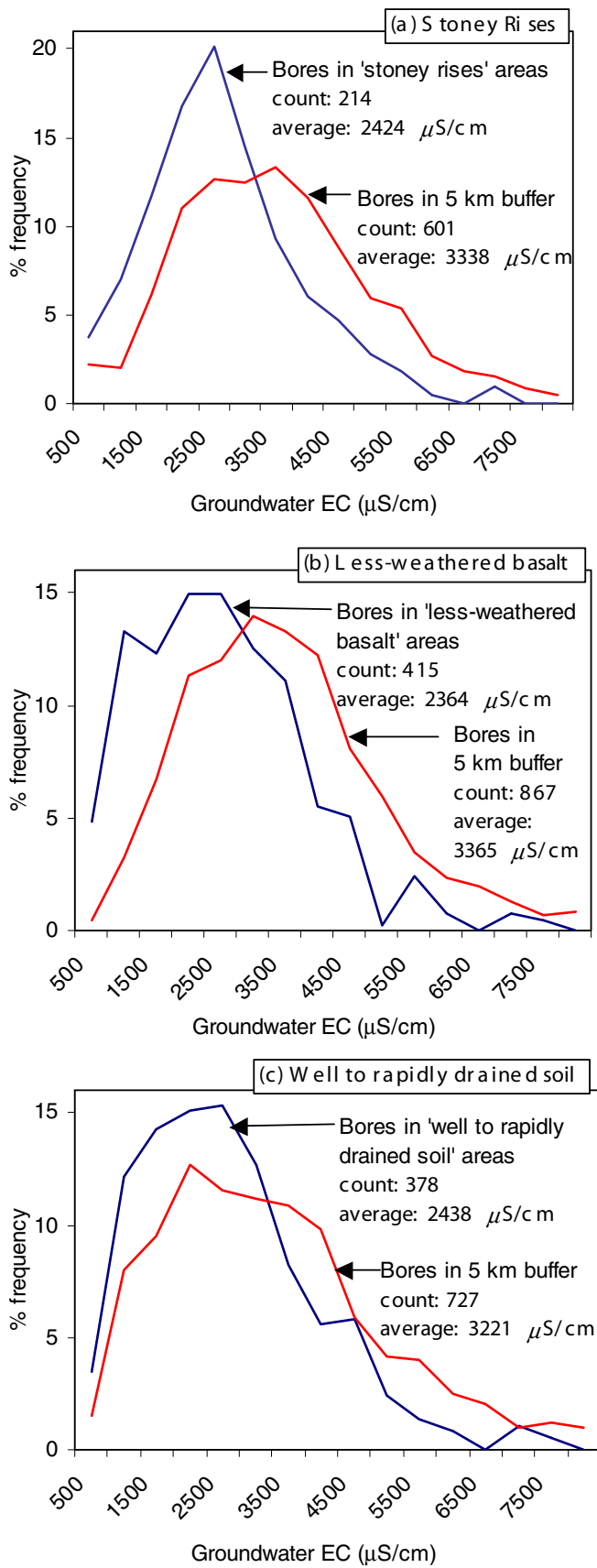


Fig. 11 Variation of groundwater EC values according to distance from a preferential recharge area (test site shown in Fig. 8b)

Recharge

The major preferential recharge areas mapped are synonymous with areas comprising relatively undeveloped weathered profiles (low clay/soil content), as reflected by the soil classes, airborne radiometric data and stoney rises (Fig. 10d). The compatibility between the hydraulic properties at the surface and the underlying lithology will ultimately determine whether these areas mapped as increased infiltration actually translate into preferential recharge areas. The correlation between preferential recharge areas and relatively low groundwater EC (Fig. 12) indicates that the unsaturated zone profiles do not inhibit the infiltration of rainfall to the water table.

The rainfall distribution map (Fig. 2) should also be taken into account when identifying areas of preferential recharge. The strong N-S rainfall gradient of ~4 mm/km, with annual rainfall varying from 500 to 900 mm/year, implies greater recharge fluxes in the south. Therefore, the term, preferential recharge, as opposed to recharge, is only pertinent when comparing recharge rates along latitudes.



◀ **Fig. 12** Distribution of groundwater EC values for bores located within and outside (5-km buffer) of **a** stoney rises, **b** less-weathered basalt and **c** well to rapidly drained soil areas in the southern region of the basalt aquifer

Uncertainties

Uncertainties inevitably exist in mapping dynamic hydrogeological processes across a ~11,500 km² surface area of the basalt aquifer. These include both temporal and spatial variability. This regional mapping should be ground-truthed for decision making on a local scale. The mapping identifies the spatial extent of processes occurring; however, it does not represent annual net influx and outflux. Temporal variations for the recharge and discharge areas includes hydraulic gradient reversal between wetlands/streams and groundwater (Weaver et al. 2004) due to either long-term impacts from land use or climate change, or due to the seasonal variability in rainfall throughout the year (Fig. 2). For example, a previous investigation in the study area correlated the change in land use (replacement of deep-rooted perennial native vegetation with shallow-rooted annual crops) with increased river salinity (Versace et al. 2005), potentially due to increased groundwater discharge. The large seasonal variations in rainfall, particularly in the southern region, also imply that wetlands and rivers may act as recharge areas during the wetter seasons and that potential recharge areas or even preferential recharge areas during dry periods may act as discharge areas. In areas mapped as both preferential recharge and discharge areas by the surface/subsurface indicators (Table 3), the presence of relatively undeveloped weathering profiles results in rapid infiltration during rainfall, and the shallow depth to water table (<5 m) results in groundwater discharge via transpiration or evaporation during dry periods. Analysis of on-ground and remotely sensed time-series data would be an effective way to constrain the long-term and seasonal variability of the discharge and recharge dynamics.

The uncertainties in mapping the spatial distribution of any hydrogeological process relates to the compatibility between the scale of the processes occurring, and the resolution of the mapping technique (Woods 2006). For example, the geomorphology of the basalt terrain results in break of slope at the edges of flows, at the sides of volcanoes and along incised drainage systems. Groundwater discharge at these break-of-slope sites can often be subtle and can occur over very small areas (few square metres). Therefore a limitation in using the break-of-slope topographic indicator in this study was the coarser DEM resolution (Table 1). The technique may better suit regions where there are larger-scale changes in the topographic relief.

Any small-scale variations in catchment properties controlling recharge and discharge processes will present significant challenges in mapping the spatial distributions across a regional area. Changes in topography and soil infiltration capacities can result in small-scale spatial variations in the recharge/discharge relationship. For example, finding techniques with the appropriate spatial resolutions to map preferential recharge pathways in dual porosity systems is complex due to the spatial

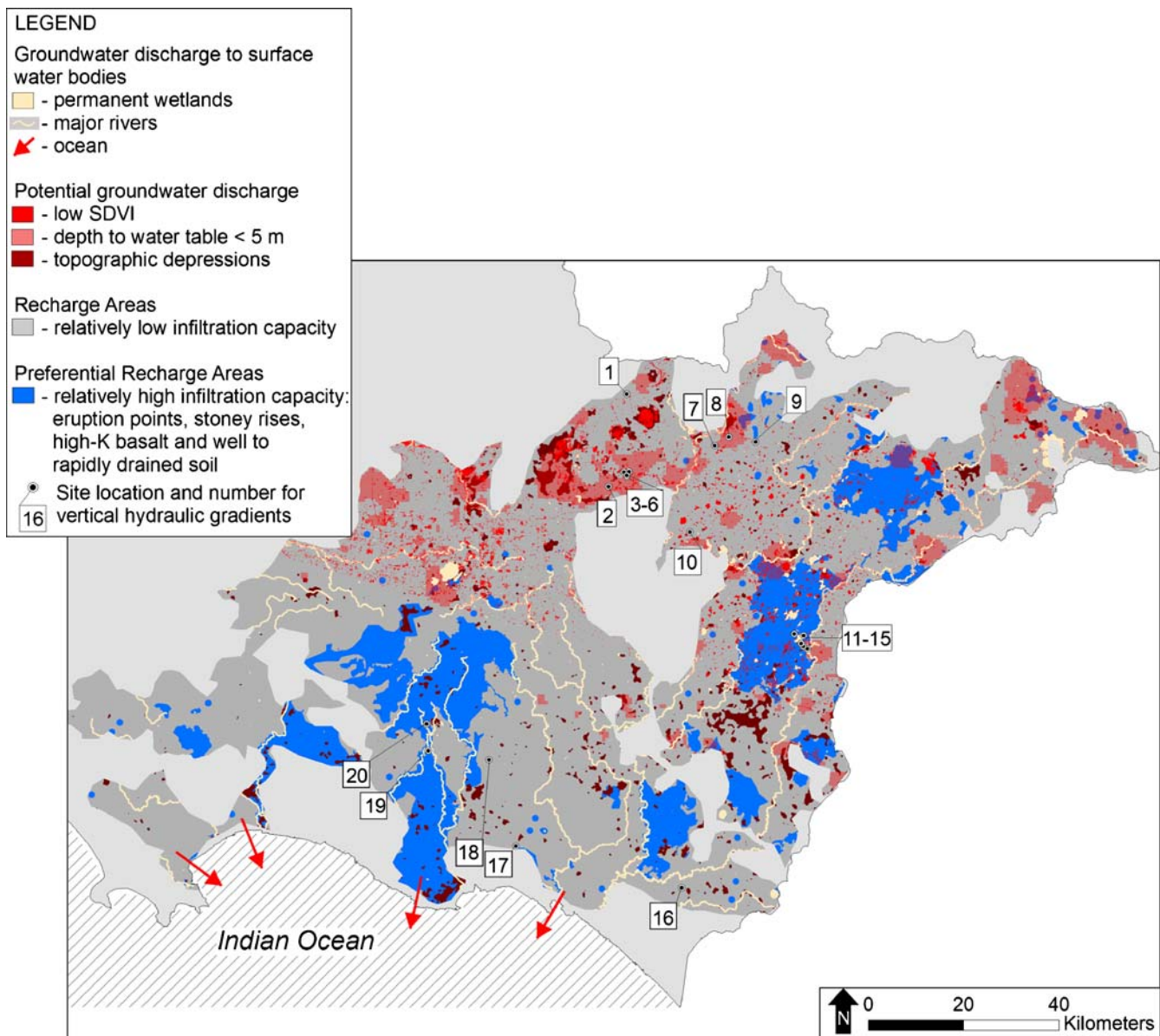


Fig. 13 Integrated map of groundwater discharge and preferential recharge areas. The discharge processes are separated by colour into indicators that highlight groundwater flow to surface water bodies, and indicators of potential discharge areas. Recharge areas are divided into regions of relatively low and relatively high (preferential recharge) infiltration capacity (grey and blue respectively). Also shown are the site numbers for nested bores used to calculate vertical hydraulic gradients (Table 3)

heterogeneity of active fractures (Sander et al. 1996; Tam et al. 2004). In this study, however, the recharge process is predominantly affected by the thickness of the weathered profile, which can be mapped at the catchment scale due to smaller spatial variability compared with fracture networks.

Applications

By identifying areas of groundwater recharge and discharge the spatial extent of these processes can be used to define boundary conditions and spatial variability of fluxes in numerical modelling (Lubczynski and Gurwin 2005). Figure 13 shows the complexity of the spatial distribution of recharge and discharge processes for the study area. Synergistic techniques, like the one proposed, can support

spatio-temporal flux redistribution as input for numerical groundwater models. In such models, the uncertainty of recharge/discharge allocation is still verified against the complex water-balance solution available in any distributed numerical groundwater model (Facchi et al. 2004; Bogena et al. 2005).

The recharge and discharge rates are affected by evaporation and transpiration (Goodrich et al. 2000). Prospective research work in the study area could investigate the use of recently developed evapotranspiration mapping techniques, e.g. energy balance models (Su 2006), to better constrain recharge and discharge rates. For groundwater evapotranspiration assessment in arid and semi-arid zones, that method can require an external calibration data source for rescaling of the remote sensing based energy balance output (Brunner et al. 2004;

Table 3 Average vertical hydraulic gradients for shallow nested bores (location shown in Fig. 13)

Site number	Average vertical hydraulic gradient ^a	Bore depths (m)	Time period		Average depth to water table (m)	Predicted process ^b	Mapped process	Indicator used ^c
			From	To				
1	0.006	20.0	48.0	Jun-1992	Aug-2003	Recharge	Recharge	Not a discharge area
2	0.032	5.0	17.0	Apr-1997	Mar-2003	Discharge	Discharge	SDVI and dtw <5 m
3	0.053	4.1	20.2	Mar-1990	May-2002	Discharge	Discharge	SDVI
4	0.007	5.2	19.0	May-1990	Aug-2003	Discharge	Discharge	dtw <5 m
5	0.015	9.3	19.2	Mar-1990	Aug-2003	Recharge	Recharge	Not a discharge area
6	0.030	12.4	22.7	Mar-1990	Aug-2003	Recharge	Recharge	Not a discharge area
7	0.006	20.0	29.5	Aug-1992	Aug-2003	Recharge	Recharge	Not a discharge area
8	0.004	11.0	40.0	Sep-1992	Aug-2003	Discharge	Discharge	dtw <5 m
9	0.003	18.0	38.0	Sep-1992	Aug-2003	Recharge	Recharge	Not a discharge area
10	0.012	17.0	53.0	Dec-1988	Aug-2003	Recharge	Recharge	Not a discharge area
11	0.003	7.0	22.0	Sep-1991	Aug-2003	Recharge	Preferential recharge or discharge	Stoney rises, high-K basalt, soil drainage and SDVI
12	0.016	16.0	37.0	Sep-1991	Aug-2003	Recharge	Preferential recharge	Soil drainage
13	0.010	6.0	26.0	Aug-1991	Aug-2003	Discharge	Preferential recharge	Soil drainage, SDVI and dtw <5 m
14	0.034	10.5	21.0	Apr-1995	Aug-2003	Recharge	Preferential recharge or discharge	Soil drainage and dtw <5 m
15	0.033	10.0	18.0	Oct-1991	Aug-2003	Discharge	Discharge	dtw <5 m
16	0.047	19.0	57.0	Nov-2000	Nov-2003	Recharge	Recharge	Not a discharge area
17	0.002	29.0	47.0	Nov-2000	Nov-2003	Recharge	Recharge	Not a discharge area
18	0.024	11.1	26.7	May-1996	Mar-2003	Recharge	Recharge	Not a discharge area
19	0.053	8.0	24.0	Aug-1992	Nov-2003	Recharge	Preferential recharge	Stoney rises, high-K basalt and soil drainage
20	0.461	8.0	47.0	Aug-1992	Nov-2003	Recharge	Preferential recharge	Stoney rises, high-K basalt and soil drainage

^a Calculated using bore depths (bottom of screen interval)

^b Upward gradient + depth to water table < 5 m = discharge area, otherwise predicted recharge area

^c dtw depth to water-table

Lubczynski and Gurwin 2005). However, for transpiration assessment in dry conditions, a more direct method of up-scaling of sap flow measurements (Cermak et al. 2004) may provide more reliable results (Lubczynski and Gurwin 2005). To distinguish between evapotranspiration processes affecting water in the unsaturated or the saturated zone is also essential. By defining the spatial extent of groundwater discharge areas, it is one step toward defining zones with certain evapotranspiration flux from the saturated zone and areas with certain recharge flux to the saturated zone.

The mapping of recharge and discharge areas is integral to managing water resources and understanding salinisation processes. In semi-arid environments, increased groundwater salinity often reflects evapotranspiration directly from the saturated zone or during recharging rainfall, rather than reflecting accumulative water–rock interaction along flow paths. Groundwater flow to the surface, and increased evaporation in these areas, can result in the degradation of water and land resources (McFarlane and Williamson 2002; Cartwright et al. 2004). The recharge map also presents information on shallow zone infiltration. The recharge regions outside the preferential recharge areas, as shown in Fig. 13, have relatively low infiltration capacities. The relatively slow recharge rates in these areas can result in increased evapotranspiration, thereby resulting in increased groundwater salinity (Herczeg et al. 2001).

Information from the recharge and discharge map can be employed by local catchment managers to help define actions for salinity mitigation, and the protection of groundwater dependant ecosystems. Secondary salinity processes, caused by land clearing after European settlement, is widespread across southern Australia. The modification of the water budget due to increased recharge after deforestation has resulted in rising water tables (Allison et al. 1990), and therefore increased groundwater salinity and discharge. Salinity mitigation programs commonly involve tree plantations to decrease recharge and/or increase discharge, thereby lowering water tables (Benyon et al. 2006; Falkiner et al. 2006). The challenge in introducing these schemes is maintaining primary discharge areas (groundwater dependant ecosystems), whilst reducing the affects of secondary saline discharge areas. Therefore tree plantations should be targeted around secondary saline discharge areas. Salinity mitigation programs should also incorporate the results from recharge mapping, so that tree plantations are restricted to areas outside of preferential recharge zones. Recharge via preferential recharge areas maintains a fresh groundwater resource, whilst the introduction of tree plantations would reduce the fresh recharge flux and increase groundwater salinity via transpiration (Leaney et al. 2005).

Conclusions

This study provides an example of linking surface features with recharge and discharge processes by incorporating GIS and remote-sensing mapping techniques. The approach

requires (1) knowledge of local hydrogeological processes occurring to choose appropriate surface/subsurface indicators, (2) adequate remote sensing and GIS techniques, as well as necessary datasets, to map these indicators, and (3) validation of the results at test sites and at the catchment scale. The systematic approach presented in this study provides a framework for mapping recharge and discharge areas across catchments. Although the selection of surface indicators is site-specific, the presented methodology and application guidelines are widely applicable.

The surface indicators of recharge and discharge should be relevant to the dominant processes occurring and have the capacity to identify these. In this example, preferential recharge and discharge areas occur at a scale that could be mapped for the ~11,500 km² surface area of the basalt aquifer. Groundwater discharge areas were best identified by mapping areas of relatively low variability of the vegetation activity. Preferential recharge areas were effectively identified by mapping areas of relatively high shallow zone infiltration rates using surface characteristics of the basalt aquifer. Therefore, groundwater discharge areas were identified by mapping the affects of discharge on surface features (vegetation), whereas preferential recharge areas were identified by mapping surface feature controls on recharge rates (infiltration).

Uncertainties in mapping discharge and recharge relations across large areas include the temporal variability, affected by both seasonal and long-term (e.g. climate and land-use) changes, and small-scale variations in the controls on preferential flow. However, by spatially defining the preferential recharge and discharge areas using GIS and remote-sensing mapping techniques, the resolution and extent of information is enhanced for the regional catchment, and, therefore, new hydrogeological information is provided for numerical modelling, water-budget analysis, and salinity mitigation programs.

Acknowledgements This study was funded by the Australian National Action Plan (NAP). The authors also wish to acknowledge input from researchers at Deakin (Frank Stagnitti and Daniel Ierodionou), La Trobe (Darren Bennetts and Matthias Raiber), Melbourne (Bernie Joyce), and Monash (Ray Cas) Universities, and the comments from the guest editor and reviewers.

References

- Al-Adamat RAN, Foster IDL, Baban SMJ (2003) Groundwater vulnerability and risk mapping for the basaltic aquifer of the Azraq basin of Jordan using GIS, remote sensing and DRASTIC. *Appl Geogr* 23:303–324
- Allison GB, Cook PG, Barnett SR, Walker GR, Jolly ID, Hughes MW (1990) Land clearance and river salinisation in the western Murray Basin, Australia. *J Hydrol* 119:1–20
- Bastiaanssen WGM, Molden DJ, Makin IW (2000) Remote sensing for irrigated agriculture: examples from research and possible applications. *Agric Water Manage* 46:137–155
- Batelaan O, De Smedt F, Triest L (2003) Regional groundwater discharge: phreatophyte mapping, groundwater modelling and impact analysis of land-use change. *J Hydrol* 275:86–108
- Bennetts DA, Webb JA (2004) Processes affecting groundwater quality in a basalt aquifer system in southern Australia. *Proceedings of the Eleventh International Symposium on*

- Water-Rock Interaction WRI-11, June 2004, Saratoga Springs, NY, pp 347–351
- Bennetts DA, Webb JA, Gray CM (2003) Distribution of Plio-Pleistocene basalts and regolith around Hamilton, western Victoria, and their relationship to groundwater recharge and discharge. Proceedings from Advances in Regolith, CRC LEME, Perth, Australia, pp 11–15
- Bennetts DA, Webb JA, Stone DJM, Hill DM (2006) Understanding the salinisation process for groundwater in an area of south-eastern Australia, using hydrochemical and isotopic evidence. *J Hydrol* 323:178–192
- Benyon RG, Theiveyanathan S, Doody TM (2006) Impacts of tree plantations on groundwater in south-eastern Australia. *Aust J Bot* 54:181–192
- Bierwirth PN, Welsh WD (2000) Delineation of recharge beds in the Great Artesian Basin using airborne gamma-radiometrics and satellite remote sensing. Report for the National Landcare Program, Bureau of Rural Sciences, Canberra, Australia, p 33
- Bobba AG, Bukata RP, Jerome JH (1992) Digitally processed satellite data as a tool in detecting potential groundwater flow systems. *J Hydrol* 131:25–62
- Bogena H, Kunkel R, Schöbel T, Schrey HP, Wendland F (2005) Distributed modeling of groundwater recharge at the macro-scale. *Ecol Model* 187:15–26
- Brunner P, Bauer P, Eugster M, Kinzelback W (2004) Using remote sensing to rationalize local precipitation recharge rates obtained from the chloride method. *J Hydrol* 294:241–250
- Cartwright I, Weaver TR, Fulton S, Nichol C, Reid M, Cheng X (2004) Hydrogeochemical and isotopic constraints on the origins of dryland salinity, Murray Basin, Victoria, Australia. *Appl Geochem* 19:1233–1254
- Cermak J, Kucera J, Nadezhdina N (2004) Sap flow measurements with some thermodynamic methods, flow integration within trees and scaling up from sample trees to entire forest stands. *Trees* 18:529–546
- Dehaan RL, Taylor GR (2002) Field-derived spectra of salinized soils and vegetation as indicators of irrigation-induced soil salinization. *Remote Sens Environ* 80:406–417
- Environmental Systems Research Institute (ESRI) (2005) ArcGIS 9.0. ESRI, Redlands, CA
- Facchi A, Ortuani B, Maggi D, Gandolfi C (2004) Coupled SWAT-groundwater model for water resources simulation in irrigated alluvial plains. *Environ Model Softw* 19:1053–1063
- Falkiner RA, Nambiar EKS, Polglase PJ, Theiveyanathan S, Stewart LG (2006) Root distribution of *Eucalyptus grandis* and *Corymbia maculata* in degraded saline soils of south-eastern Australia. *Agrofor Syst* 67:279–291
- Fritch TG, McKnight CL, Yelderman JC Jr, Arnold JG (2000) Environmental auditing: an aquifer vulnerability assessment of the Paluxy Aquifer, central Texas, USA, using GIS and a modified DRASTIC approach. *Environ Manage* 25(3):337–345
- Goodrich DC, Scott R, Qi J, Goff B, Unkrich CL, Moran MS, Williams D, Schaeffer S, Snyder K, MacNish R, Maddock T, Pool D, Chehbouni A, Cooper DI, Eichinger WE, Shuttleworth WJ, Kerr Y, Marssett R, Ni W (2000) Seasonal estimates of riparian evapotranspiration using remote and in situ measurements. *Agric For Meteorol* 105:281–309
- Gowing JW, Konukcu F, Rose DA (2006) Evaporative flux from a shallow water table: the influence of a vapour-liquid phase transition. *J Hydrol* 321:77–89
- Herczeg AL, Dogramaci SS, Leaney FW (2001) Origin of dissolved salts in a large, semi-arid groundwater system: Murray Basin, Australia. *Mar Freshw Res* 52:41–52
- Hoffmann J (2005) The future of satellite remote sensing in hydrogeology. *Hydrogeol J* 13:247–250
- Howari FM (2003) The use of remote sensing data to extract information from agricultural land with emphasis on soil salinity. *Aust J Soil Res* 41:1243–1253
- Ierodiaconou D, Laurenson L, Leblanc M, Stagnitti F, Duff G, Salzman S, Versace V (2005) The consequences of land use change on nutrient exports: a regional scale assessment in south-west Victoria, Australia. *J Environ Manage* 74:305–316
- ITT Visual Information Solutions (2005) ENVI 4.2, <http://www.itervis.com>. Cited 8 November 2006
- Jackson TJ (2002) Remote sensing of soil moisture: implications for groundwater recharge. *Hydrogeol J* 10:40–51
- Joyce EB (1999) A new regolith landform map of the western Victorian volcanic plains, Victoria, Australia. In: Taylor G, Pain C (eds) *Regolith '98, Australian regolith and mineral exploration: new approaches to an old continent*. Proceedings, 3rd Australian Regolith Conference, Kalgoorlie, 2–9 May 1998, CRC LEME, Perth, pp 117–126
- Kishel HF, Gerla PJ (2002) Characteristics of preferential flow and groundwater discharge to Shingobee Lake, Minnesota, USA. *Hydrol Process* 16:1921–1934
- Leaney FW, Mustafa S, Lawson J (2005) Salt accumulation and water balance under different land use in Bakers Range area. CSIRO Land and Water Science Report 05/06, CSIRO, Clayton South, Australia
- Leblanc M, Leduc C, Razack M, Lemoalle J, Dagorne D, Mofor L (2003a) Application of remote sensing and GIS for groundwater modelling of large semiarid areas: example of the Lake Chad Basin, Africa. *Hydrology of Mediterranean and Semiarid Regions Conference, Montpieller, France, April 2003, IAHS (Red Books Series), Wallingford, UK, no. 278, pp 186–192*
- Leblanc M, Razack M, Dagorne D, Mofor L, Jones C (2003b) Application of Meteosat thermal data to map soil infiltrability in the central part of the Lake Chad basin, Africa. *Geophys Res Lett* 30(19):1998. DOI 10.1029/2003GL018094
- Lubczynski MW, Gurwin J (2005) Integration of various data sources for transient groundwater modelling with spatio-temporally variable fluxes: Sardon study case, Spain. *J Hydrol* 306:71–96
- McFarlane DJ, Williamson DR (2002) An overview of water logging and salinity in southwestern Australia as related to the 'Ucarro' experimental catchment. *Agric Water Manage* 53:5–29
- Meijerink AMJ (1996) Remote sensing applications to hydrology: groundwater. *Hydrol Sci* 41(4):549–561
- Metternicht G, Zinck JA (1997) Spatial discrimination of salt- and sodium-affected soil surfaces. *Int J Remote Sens* 18(12):2571–2586
- Metternicht GI, Zinck JA (2003) Remote sensing of soil salinity: potentials and constraints. *Remote Sens Environ* 85:1–20
- Moore ID, Grayson RB, Landson AR (1991) Digital terrain modelling: a review of hydrological, geomorphological, and biological applications. *Hydrol Process* 5:3–30
- Munro M (2000) Salinity discharge in the Glenelg Hopkins CMA region. Department of Natural Resources and Environment, Casterton, Australia, 29 pp
- Rango A, Shalaby AI (1998) Operational applications of remote sensing in hydrology: success, prospects and problems. *Hydrol Sci* 43(6):947–968
- Salama R (1998) Physical and chemical techniques for discharge studies, part 1. In: Zhang L, Walker G (eds) *The Basics of recharge and discharge*, CSIRO, Clayton, Australia. pp 1–29
- Salama R, Tapley I, Ishii T, Hawkes G (1994) Identification of areas of recharge and discharge using Landsat-TM satellite imagery and aerial photography mapping techniques. *J Hydrol* 162:119–141
- Salama R, Hatton T, Dawes W (1999) Predicting land use impacts on regional scale groundwater recharge and discharge. *J Environ Qual* 28:446–460
- Sander P, Chesley MM, Minor TB (1996) Groundwater assessment using remote sensing and GIS in a rural groundwater project in Ghana: lessons learned. *Hydrogeol J* 4(3):40–49
- Sener E, Davraz A, Ozcelik M (2005) An integration of GIS and remote sensing in groundwater investigations: a case study in Burdur, Turkey. *Hydrogeol J* 13:826–834
- Spies B, Woodgate P (2005) Salinity mapping methods in the Australian context. Prepared for the Natural Resource Management Ministerial Council through Land and Water Australia and the National Dryland Salinity Program, Canberra, Australia
- Su Z (2006) Estimation of the surface energy balance. In: Anderson MG (ed) *Remote sensing, part 5. Encyclopedia of hydrological sciences*, Wiley, New York. DOI 10.1002/0470848944.hsa068
- Tam VT, De Smedt F, Batelaan O, Dassargues A (2004) Study on the relationship between lineaments and borehole specific capacity in a fractured and karstified limestone area in Vietnam. *Hydrogeol J* 12:662–673

- Tcherepanov EN, Zlotnik VA, Henebry GM (2005) Using Landsat thermal imagery and GIS for identification of groundwater discharge into shallow groundwater-dominated lakes. *Int J Remote Sens* 26(17):3649–3661
- Thorburn PJ, Walker GR, Woods PH (1992) Comparison of diffuse discharge from shallow water tables in soils and salt flats. *J Hydrol* 136:253–274
- UNEP (1992) World atlas of desertification. Arnold, London, 69 pp
- Versace V, Ierodiaconou D, Salzman S, Stagnitti F, Leblanc M, Boland A, Laurenson L, March T, Thwaites L (2005) Multivariate modelling of land use on in-stream salinity over multiple spatial scales. In: Water resources management III. Series: Progress in Water resources, vol 1, Wessex Institute of Technology, UK
- Vieux BE (1995) DEM aggregation and smoothing effects on surface runoff modeling, Chap 15. In: Lyon JG, McCarthy J (eds) Wetland and environmental applications of GIS, Lewis, Boca Raton, FL
- Weaver TR, Bush A, Singh T, Cartwright I, Irvine E (2004) Models for development of dryland salinity, Murray Basin, Australia. In: Wanty R, Seal II R (eds) Proceedings water–rock interaction 11, Balkema, Lisse, The Netherlands, pp 519–522
- Wilson JP, Gallant JC (2000) Digital terrain analysis, chap 1.. In: Wilson JP, Gallant JC (eds) Terrain analysis: principles and applications. Wiley, New York, pp 1–27
- Woods R (2006) Hydrologic concepts of variability and scale, In: Anderson MG (ed) Encyclopedia of hydrological sciences, part 1. Theory, organization and scale, Wiley, New York. DOI [10.1002/0470848944.hsa002](https://doi.org/10.1002/0470848944.hsa002)